Detection of the ~~freezing~~ melting level with polarimetric weather radar

Daniel Sanchez-Rivas and Miguel A Rico-Ramirez

Department of Civil Engineering, University of Bristol, Bristol, BS8 1TR, United Kingdom

Correspondence: Daniel Sanchez-Rivas (d.sanchezrivas@bristol.ac.uk)

Abstract. Accurate estimation of the ~~Freezing Level (FL~~Melting Level (ML) is essential in radar rainfall estimation to mitigate the bright band enhancement, ~~to~~ classify hydrometeors, ~~to~~ correct for rain-attenuation~~and to~~, and calibrate radar measurements. ~~Here we present~~ This paper presents a novel and robust ~~FL estimation algorithm that can be applied to~~ ML detection algorithm based on either Vertical Profiles (VPs) or Quasi-Vertical Profiles (QVPs) built from operational polarimetric weather radar

5   scans. The algorithm depends only on data collected by the radar itself ~~,~~ and it is based on the ~~detection of strong gradients within the profiles and relies on the~~ combination of several polarimetric ~~variables. The VPs and QVPs of Z_H showed a good similarity in the profiles ($r \approx 0.7$) even though the QVPs are built from low-elevation angles~~radar measurements to generate an enhanced profile with strong gradients related to the melting layer. The algorithm is applied to one year of rainfall events ~~and validated using measured FLs from~~ that occurred over South East England and the results were validated using radiosonde

10   data. ~~The results demonstrated that combining the profiles~~ After evaluating all possible combinations of polarimetric radar measurements, the algorithm achieves the best ML detection when combining VPs of Z_H, ρ_{HV} and the gradient of the velocity V ~~showed the best FL estimation performance when using VPs, whereas combining the~~ whereas for QVPs, combining profiles of Z_H, ρ_{HV} and Z_{DR} ~~showed the best FL estimation performance when using QVPs. The VP computed from the gradient of the velocity showed to be extremely valuable in the FL estimation when using VPs. The errors in the FL estimation using~~

15   ~~either VPsor QVPs are within 250 m~~ produces the best results, regardless of the type of rain event. The root mean square error in the ML detection compared to radiosonde data is ~ 200 m when using VPs, and ~ 250 m when using QVPs.

1 Introduction

~~Accurate detection of the Freezing Level (FL) is important for meteorological and hydrological applications of weather radar rainfall measurements. The FL represents the height in the free atmosphere at which~~ The Melting Level (ML) is defined as the

20   altitude of the ~~measured temperature is~~ $0°C$ ~~and it is crucial in radar rainfall applications because it is~~ constant-temperature surface (American Meteorological Society, 2021b). It is located at the top of the melting layer, which represents the altitude interval where the transition between solid and liquid precipitation ~~which show different backscattering properties.~~ occurs (American Meteorological Society, 2021a). As the melting layer generates distinctive weather radar signatures, e.g., the well-known radar Bright Band (BB), its detection is important for meteorological and hydrological applications of weather radar rainfall

25   measurements.

When using weather radar data for quantitative precipitation estimation (QPE), it is necessary to apply several corrections to the ~~reflectivity~~ radar data before they can be converted into estimates of rainfall rates (Dance et al., 2019; Hong and Gourley, 2015; Mittermaier and Illingworth, 2003). For instance, corrections due to the ~~radar Bright Band (BB)~~ BB are necessary as ~~the BB is~~ it generates a region of enhanced reflectivity ~~located below the FL~~ due to the melting of hydrometeors, ~~that can~~ which

30   cause an overestimation of rainfall rates (Cheng and Collier, 1993; Rico-Ramirez and Cluckie, 2007). In this case, the ~~location of the FL~~ ML location is necessary to ~~locate the BB to~~ determine the location of the BB and apply the required algorithms to mitigate the effects of this error source in radar QPE (Sánchez-Diezma et al., 2000; Smyth and Illingworth, 1998; Vignal et al., 1999). Above the BB, a correction for the variation of the Vertical Profile of Reflectivity (VPR) is also required, especially during stratiform precipitation, where the reflectivity of snow and ice particles decreases with height. In the UK, VPR corrections

35   to radar data are ~~performed by using the FL~~ usually performed using the ML computed from a numerical weather prediction (NWP) model~~,~~ (Harrison et al., 2000; Mittermaier and Illingworth, 2003) assuming a ~~700 m BB tickness. In fact~~ constant BB thickness. Additionally, most of the radar-based hydrometeor classification algorithms require some form of separation between liquid and solid precipitation, hence the reliability of accurate identification of the ~~FL~~ ML (Hall et al., 2015; Kumjian, 2013a; Park et al., 2009). Even more, the attenuation of the radar signal at higher frequencies (C, X, Ka and W bands) is a

40   significant error source for radar QPE. Attenuation correction algorithms are applied in the rain region, ~~which again~~ and this requires knowledge of the height of the ~~FL (Bringi et al., 1990; Islam et al., 2014; Park et al., 2005; Rico-Ramirez, 2012)~~ ML (Bringi et al., 2001; Islam et al., 2014; Park et al., 2005; Rico-Ramirez, 2012).

~~Knowledge of the FL is also useful to calibrate radar measurements. For instance, the differential reflectivity (Z_{DR}) is a variable that is subject to calibration errors, and the FL location is really helpful to quantify the bias of Z_{DR} and mitigate errors in rain~~

45   ~~rates computed with the reflectivity (Z_H) and Z_{DR} (Richardson et al., 2017). Depending on the radar scanning strategy, radar networks around the world have implemented operational algorithms for Z_{DR} calibration. Gorgucci et al. (1999) developed a method where vertical-looking radar observations in light rain are used to calibrate Z_{DR} given that the shape of raindrops seen by the radar at $90°$ elevation is nearly circular and therefore vertical Z_{DR} measurements in light rain should be around 0 dB. As vertical measurements sometimes are not available due to mechanical radar restrictions, Ryzhkov et al. (2005),~~

50   ~~Bechini et al. (2008), Gourley et al. (2009), among others, developed algorithms for Z_{DR} calibration analysing the inter-dependency between Z_{DR} and other polarimetric variables for several targets with a known -intrinsic value of Z_{DR}, e.g. rain medium or dry snow, hence the importance of the FL estimation.The development of polarimetric weather radar technology has allowed measuring the size and thermodynamic phase of precipitation particles. This has enabled the development of algorithms to estimate the FL directly from radar measurements based primarily on the premise that the freezing level and the melting layer~~

55   ~~(ML) are linked, as the latter describes the transition between ice /snow and water particleson the atmosphere, which show distinctive radar signatures. Using~~ There is a large number of papers that show the relationship between the BB enhancement and the melting layer. Klaassen (1988) modelled the melting layer and found that the BB enhancement in the radar reflectivity (Z_H) is related to the density of the ice particles. Based on vertically pointing radar measurements, Fabry and Zawadzki (1995) analysed the dependency of the BB on the precipitation intensity and ~~proved~~ confirmed the relationship between the radar

60   BB signatures and the melting of snowflakes in stratiform precipitation. ~~Klaassen (1988) modelled the melting layer using~~

~~high-resolution Doppler radar data and found that the BB is related to the density of the ice particles for Z_H and mean Doppler velocity.~~ White et al. (2002) introduced an algorithm based on Doppler wind profiling radar scans for detecting the BB height~~,~~; their results showed ~~that the~~ a correlation between the melting layer and the peaks of the gradients of Z_H ~~,~~ and the Doppler vertical velocity (V)~~and the ML are correlated. Similarly, Baldini and Gorgucci (2006) integrated~~. Recently, the development of polarimetric weather radar has allowed measuring the size and thermodynamic phase of precipitation particles, which has improved the identification of the melting layer. For instance, Baldini and Gorgucci (2006) used the differential reflectivity (Z_{DR}) and the differential propagation phase (Φ_{DP}) taken at vertical incidence to the analysis of the ML. They showed that the standard deviation of these measurements along with Z_H and V are useful for the identification of the ML using C-Band radar data.

~~There are different algorithms available in the literature to estimate the FL using polarimetric radar measurements. Because the BB is characterised by a region of enhanced values of Z_H and linear depolarisation ratio (LDR) and depressions in the correlation coefficient (ρ_{HV}), this has been exploited by different authors to get an estimation of the FL. Brandes and Ikeda (2004) developed an empirical procedure based primarily on idealised profiles of Z_H, LDR and ρ_{HV} that are compared with observed profiles to estimate the height of the FL; in the last step of their procedure, the height of the FL is refined using equations related to the precipitation intensity. Giangrande et al. (2008) analysed the correspondence between maxima of Z_H, Z_{DR} and minima in ρ_{HV} to estimate the boundaries of the melting layer (ML) using conventional Plan Position Indicator (PPI) radar scans . The algorithm is tailored for scans with elevations angles between $4°$ and $10°$. Later, Boodoo et al. (2010) proposed an adaptation of this algorithm, varying the scan elevation and the range of values of Z_H, Z_{DR} and ρ_{HV} making the algorithm more sensitive to less intense values of the BB~~Several algorithms to identify the melting layer using Range Height Indicator (RHI) scans have been proposed in the literature. Matrosov et al. (2007) proposed an approach to identify ~~rain and ML regions based only on the vertical profiles of ρ_{HV} from Range Height Indicator (RHI) scans~~ the melting layer based on RHI correlation coefficient (ρ_{HV}) measurements collected by an X-band radar. The method relates the depressions ~~of~~ on the ρ_{HV} profile ~~in the ML~~to the melting layer, with the disadvantage that the absence of such depressions ~~(e.g. warm and convective rain)~~ hampers the application of the algorithm. ~~Similarly,~~ Similarly, for RHI scans Wolfensberger et al. (2016) designed an algorithm that combines Z_H and ρ_{HV} to create a new vertical profile that enables the detection of ~~gradient variations on the vertical profiles, which are then~~ strong gradients related to the boundaries of the ~~ML~~melting layer. They applied this algorithm to X-band ~~polarimetric RHI~~ scans, and their results showed that the algorithm is efficient to characterise the thickness of the ~~ML~~ melting layer and as a foundation for hydrometeor classification algorithms. Based on C-band RHI scans, Shusse et al. (2011) described the shape and variation of the melting layer on different rainfall systems and provided insights into the behaviour of Z_{DR} and ρ_{HV} in convective precipitation events.

~~Operational polarimetric weather radars are not always able to perform vertical pointing scans~~Algorithms to identify the melting layer based on Plan Position Indicator (PPI) scans have also been proposed in the literature. Brandes and Ikeda (2004) developed an empirical procedure based primarily on idealised profiles of Z_H, LDR and ρ_{HV} that are compared with observed profiles to estimate the height of the freezing level; also the estimation of the freezing level height is refined using equations related to the precipitation intensity. Giangrande et al. (2008) analysed the correspondence between maxima of Z_H, ~~or RHI~~

scans to observe the vertical structure of precipitation. In this case, Z_{DR} and minima in ρ_{HV} to estimate the boundaries of the melting layer using conventional PPI radar scans. The algorithm is tailored for scans with elevations angles between $4°$ and $10°$. Later, Boodoo et al. (2010) proposed an adaptation of this algorithm, varying the scan elevation and the range of values of Z_H, Z_{DR} and ρ_{HV} making the algorithm more sensitive to less intense signatures of the melting layer.

100   As the PPI is the most common product derived from weather radars, Ryzhkov et al. (2016) proposed the Quasi-Vertical Profiles (QVPs) technique to seize the benefits of PPIs; this technique can be used ~~to~~ for monitoring the temporal evolution of precipitation and the microphysics of precipitation~~(Ryzhkov et al., 2016)~~. For instance, ~~Kumjian and Lombardo (2017) and Griffin et al. (2018) introduced new procedures for generating QVPs of the radial velocity and specific differential phase (K_{DP}) to explore the polarimetric signatures of microphysical processes within winter precipitation events at S-band frequencies.~~

105   ~~Similarly,~~ Kaltenboeck and Ryzhkov (2017) analysed the evolution of the ~~ML~~ melting layer in freezing rain events with ~~the QVP technique~~QVP signatures, demonstrating the ability of ~~the~~ QVPs to represent several microphysical precipitation features as the dendritic growth layer and the riming region~~, both of them related to the ML and FL~~. Furthermore, Kumjian and Lombardo (2017), and Griffin et al. (2018) introduced new procedures for generating QVPs of the radial velocity and specific differential phase (K_{DP}) to explore the polarimetric signatures of microphysical processes in winter precipitation events at S-band frequencies.

110   Despite the enormous benefits that QVPs bring in terms of improving our understanding of the microphysics of precipitation, there is very little research on the use of QVP-based algorithms to estimate the ~~FL~~ML. ~~Most of the algorithms mentioned above require measurements of the vertical structure of precipitation (~~Knowledge of the ML is also useful to calibrate radar measurements. For instance, Z_{DR} is prone to calibration errors. The ML location is helpful to quantify the bias of Z_{DR} and mitigate errors in rain rate algorithms that use Z_H and Z_{DR} data (Richardson et al., 2017)

115   . Depending on the radar scanning strategy, radar networks worldwide have implemented operational algorithms for Z_{DR} calibration that require knowledge of the ML. Gorgucci et al. (1999) developed a method where vertical-pointing radar observations in light rain are used to calibrate Z_{DR} given that the shape of raindrops seen by the radar at $90°$ elevation is nearly circular and therefore Z_{DR} measurements in light rain should be around 0 dB. As vertical measurements sometimes are not available due to mechanical radar restrictions, Ryzhkov et al. (2005), Bechini et al. (2008), Gourley et al. (2009), among others, developed

120   algorithms for Z_{DR} calibration analysing the inter-dependency between Z_{DR} and other polarimetric variables for several targets with a known -intrinsic value of Z_{DR}, e.g. ~~RHI scans) to estimate the FL, which might not be available in~~ rain medium or dry snow, hence the importance of the ML estimation.
Most of the algorithms mentioned above require measurements often not available from operational weather radar networks ~~. Operational weather radar networks produce volume scans at different elevation angles that allow an insightful analysis of~~

125   ~~the characteristics of the FL. Therefore, this paper presents a novel,~~ as weather radars cannot always perform vertical pointing scans or produce RHI scans to observe the vertical structure of precipitation events. Hence, this work's main objective is to present an automated, operational and robust algorithm that can accurately detect the ~~FL~~ML based on QVPs or ~~Vertical profiles (VPs) of polarimetric measurements collected from an operational C-band dual-polarisation weather radar and demonstrate its performance for different types of events. The results are compared with FL heights from the UKMO~~ VPs (Vertical Profiles)

130   collected from operational polarimetric weather radars. The algorithm outputs are validated using ML heights from high-

4

resolution radiosonde data. ~~The latter enables the analysis of the performance of QVPs and VPs on the FL estimation.~~ Note that the proposed algorithm is not intended to replace NWP-based ~~FL~~ ML estimation methods, but it is an alternative way to ~~estimate the FL~~ detect the ML when only polarimetric weather radar measurements are available. The paper is organised as follows: the next section will describe the datasets used to design and validate the algorithm. The aim of Section 3 is to examine the signatures of the melting layer on both QVPs and VPs of polarimetric variables. Section 4 provides a detailed explanation of the design of the algorithm. Results, implementation, validation and several examples of the outputs of the algorithm are presented in Section 5. Section 6 provides a discussion on the performance and implementation of the algorithm. Finally, Section 7 provides a summary of the conclusions from this work.

2   Datasets and Methods

~~The~~ Radiosonde data were used to validate the ML estimated from radar observations. The radiosonde is an instrument that is released into the atmosphere to measure several atmospheric parameters. The UK Met Office (UKMO) uses the Vaisala RS80 radiosonde model to collect upper-air observations twice a day at different locations across the UK. The ascent of the radiosonde extends to heights of approximately 10-30 km and take measurements at 2-second intervals (Met Office, 2007). The closest station to the selected radar site is the Herstmonceux station (see location in Figure 1), which provides high-resolution radiosonde information of pressure, temperature, relative humidity, humidity mixing ratio, sonde position, wind speed and wind direction. As these measurements provide insights for the ML location, the radiosonde data were processed to estimate the height of the $0°C$ Wet-Bulb Temperature to evaluate the algorithm performance.

The Chenies C-band operational weather radar located in South East England was selected for this work as it was one of the first UKMO radars upgraded with polarimetric capabilities (Norman et al., 2014)~~(see Table 1 and Figure 1)~~. The radar transmits both ~~horizontal and vertical pulses~~ horizontally and vertically polarised electromagnetic waves simultaneously and receives co-polar signals at the same ~~time, generating polarimetric measurements of~~ polarisation as that of the transmitted wave, generating measurements such as Z_H, Z_{DR}, ρ_{HV} and Φ_{DP}. ~~Doppler~~ Mean radial velocity (V) ~~information on the observed droplets is also available(Met Office, 2013).~~ measurements of the observed precipitation targets are also available; LDR measurements are also produced ~~using a special separated pulse. The scanning strategy implemented on this radar~~ for the lowest elevation scan (Met Office, 2013). The volume radar scanning strategy generates different products:

- 5 PPI scans sampled on Long Pulse (LP) mode (pulse length= $2,000\mu s$; range covered=250 km) at $0.5°$, $1°$, $2°$, $3°$ and $4°$ elevation angles with a 600 m gate resolution every 5 minutes.

- 5 PPI scans sampled on Short Pulse (SP) mode (pulse length= $500\mu s$; range covered=115 km) at $1°$, $2°$, $4°$ $6°$ and $9°$ elevation angles, every 10 minutes and same gate resolution as above.

- One SP PPI scan at vertical incidence (range covered=12 km) every 10 minutes with 75 m gate resolution.

- One PPI scan with LDR measurements every 5 minutes at the lowest elevation ($0.5°$).

5

The location and other radar characteristics are provided in Table 1 and Figure 1.
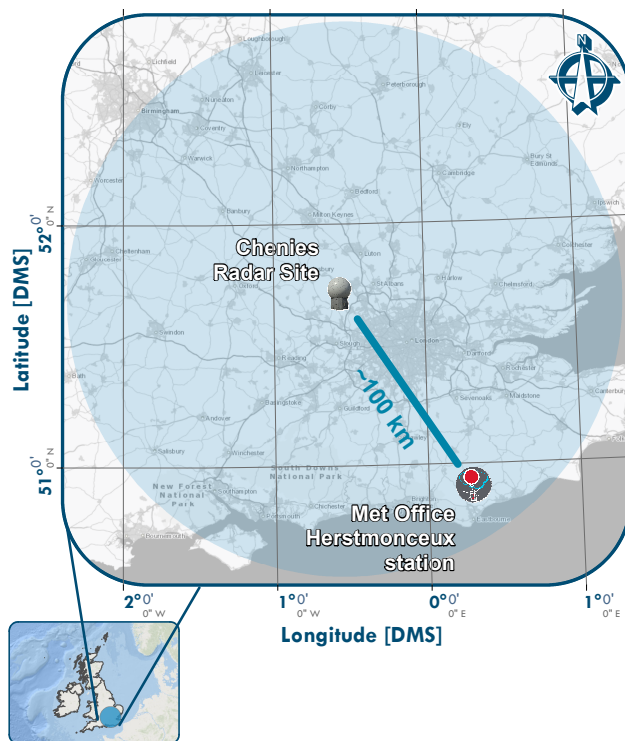

Figure 1. Location and coverage (on SP mode) of the Chenies radar and location of the Herstmonceux station.

Polarimetric scans related to precipitation events throughout 2018 were analysed for the design and evaluation of the algorithm. To reduce the probability of ground clutter contamination and beam spreading effects, only SP scans from the $4°$, $6°$, $9°$ and $90°$ elevations angles were retained for further processing. ~~A total of 94 rainfall events with visible signatures of enhancement (related to the FL) on the polarimetric variables were selected, of which 25 had a suitable temporal matching~~

Table 1. Chenies radar characteristics.

	Chenies radar
Location	~~51.6892, -0.5297~~51°41'21.1"N, 0°31'46.9"W
Wavelength	$\lambda = 5.3\ cm$
Multiple elevation scans	$0.5°$ to $90°$
Beam-width	$1.0°$
PRF	900 Hz (SP) - 300 Hz (LP)
RPM	3.6 (SP) - 1.4 (LP)

~~between the precipitation events recorded by the radar and the data collected by the radiosondes.~~ Then, a pre-processing of the raw-radar-data is carried out to discard non-meteorological echoes and construct the profiles of polarimetric variables:

– For the $4°$, $6°$ and $9°$ elevations scans, remnant clutter and anomalous propagation echoes were removed using the algorithm proposed by Rico-Ramirez and Cluckie (2008), specifically calibrated with ~~this radar data~~data from this radar. Then, following the procedure suggested by Ryzhkov et al. (2016), we generated QVPs of Z_H, Z_{DR}, ρ_{HV} and Φ_{DP} measurements. The procedure ~~suggest~~ suggests the azimuthal averaging of the polarimetric measurements at high elevation scans ($10°$-$30°$), ~~and results in height-versus-time representations of the polarimetric variables that enable the observation of the vertical structure of precipitation and the identification of distinctive ML signatures~~but such elevation angles were not available on our datasets; hence we used lower elevation angles to generate the QVPs. Although it is possible to produce time-averaged QVPs to avoid local storm effects, we decided to keep the original time resolution of the QVPs, and so we produced one QVP for each PPI scan. Details on the construction of the QVPs is provided in section 6.

– For the vertical scans, the ~~first kilometre of data~~ data related to the first kilometre above ground level (a.g.l.) is not usable due to some inherent radar limitations, e.g. the de-ionisation time of the Transmit-Receive (TR) cell (Darlington, 2019, personal communication) or clutter contamination. After discarding the data below this height, an azimuthal averaging of the polarimetric and Doppler velocity data collected at vertical incidence was performed, generating the VPs of Z_H, Z_{DR}, ρ_{HV}, Φ_{DP} and V. For the analysed radar datasets, the Spectral width variable was not available. Based on the profiles of vertical velocity [V], we propose a new variable: [$gradV$], that calculates the gradient of the $90°$ velocity profile (note that $gradV \equiv dV/dH$). This new variable accentuates the profile extremes ~~that are~~ related to the change in the hydrometeor fall velocities from ice/snow to rain. The gradient of V is computed using first-order central differences in the interior points and first-order forward or backwards differences at the boundaries; for an in-depth description of numerical differentiation and finite-differences methods see Moin (2010).

Regarding the attenuation corrections needed for Z_H and Z_{DR}, for most of the scans used in this work (especially $90°$ scans and high-elevation scans at $9°$ elevation) we observed that rain attenuation was relatively small after analysing the total differential

phase shift. Furthermore, the ML height is essential to implement rain attenuation correction algorithms. Hence, no attempt was made to correct for attenuation.

Based on the constructed VPs and QVPs, a total of 94 rainfall events with visible signatures of the melting layer on Z_H or ρ_{HV} were selected, i.e. an enhancement up to 30 dBZ on Z_H or ρ_{HV} constantly decreasing below 0.90. Also, from the total number of rain events, only 25 events observed by the radar shown a suitable temporal matching with the data collected by the radiosondes, i.e. the difference in time between measurements do not exceed 2 hours. This time window was set to minimise the impact of the variability of the height of the ML.

3 Polarimetric signatures of the melting layer

4 ~~Polarimetric signatures of the melting layer~~

~~The raw polarimetric radar data were pre-processed as described in the previous section in order to generate height-versus-time plots of~~ The VPs and QVPs of ~~all polarimetric measurements available to visualise the ML signatures of different precipitation events~~ the polarimetric measurements are displayed in height-versus-time plots. This enables the visualisation of the melting layer signatures on the radar measurements. Figure 2 ~~displays an example for a~~ depicts an stratiform rainfall event recorded between 9-10 April 2018 using VPs and QVPs ~~at~~ (9° elevation angle). It can be seen that every radar variable exhibits distinctive features that provide unique information for the identification of the melting layer ~~and the FL~~ on both, VPs and QVPs, e.g. Figures 2a-2b, and 2c-2d exhibit regions of enhanced values of Z_H (BB) and Z_{DR}, respectively, that are visible just below 2 km in height. Concurrently, Figures 2e-2f and 2g-2h show that ρ_{HV} and Φ_{DP}, are sensitive to the phase and shape of hydrometeors, while Figure 2i shows that the fall velocities of snow particles are lower compared to rain particles, which is an important feature that can be used to detect the ~~FL~~ML. Figure 2j shows the enhanced region where the transition between the fall velocities of snow and rain particles occurs in the proposed new variable $[gradV]$. The different signatures expected in the ~~ML~~ melting layer on the QVPs and VPs are explained next.

~~The~~ For comparison purposes, Figure 3 shows normalised versions of VPs and QVPs ~~are normalised to enhance the features observed in the BB and at the FL. An example of normalised polarimetric profiles related to a stratiform event~~ (scaling each profile into the range [0, ~~corresponding to different elevation angles and with the extents set for comparison purposes only, is shown in Figure 3 along with the closest-in-time radiosonde data where the temperature reaches~~ 1]) taken from the stratiform event presented in Figure 2; also, the height of the $0°C$ ~~(FL_{RS}).~~ Wet-Bulb isotherm is shown. The normalisation process intensifies the signatures of the melting layer. Note that the QVPs provide information below 1 km; this is important for the analysis of showers or events with ML at relatively low altitude.

Given that the main objective of this work is to ~~estimate the FL~~ detect the melting layer boundaries based on the geometric features of the polarimetric profiles, herein, we will try to explain ~~the enhancements that the ML bring-up into the variables~~ how the melting layer shapes the structure of the radar profiles. Figure 3 shows ~~that the enhancement~~ the presence of enhancements on the polarimetric ~~variables is~~ profiles related to the variation of the phase and concentration of the hydrometeors,~~ i. e. the ML, and the upper boundary~~. Taking the $0°C$ wet-bulb height as a reference (just below 2 km in altitude), it is feasible to associate
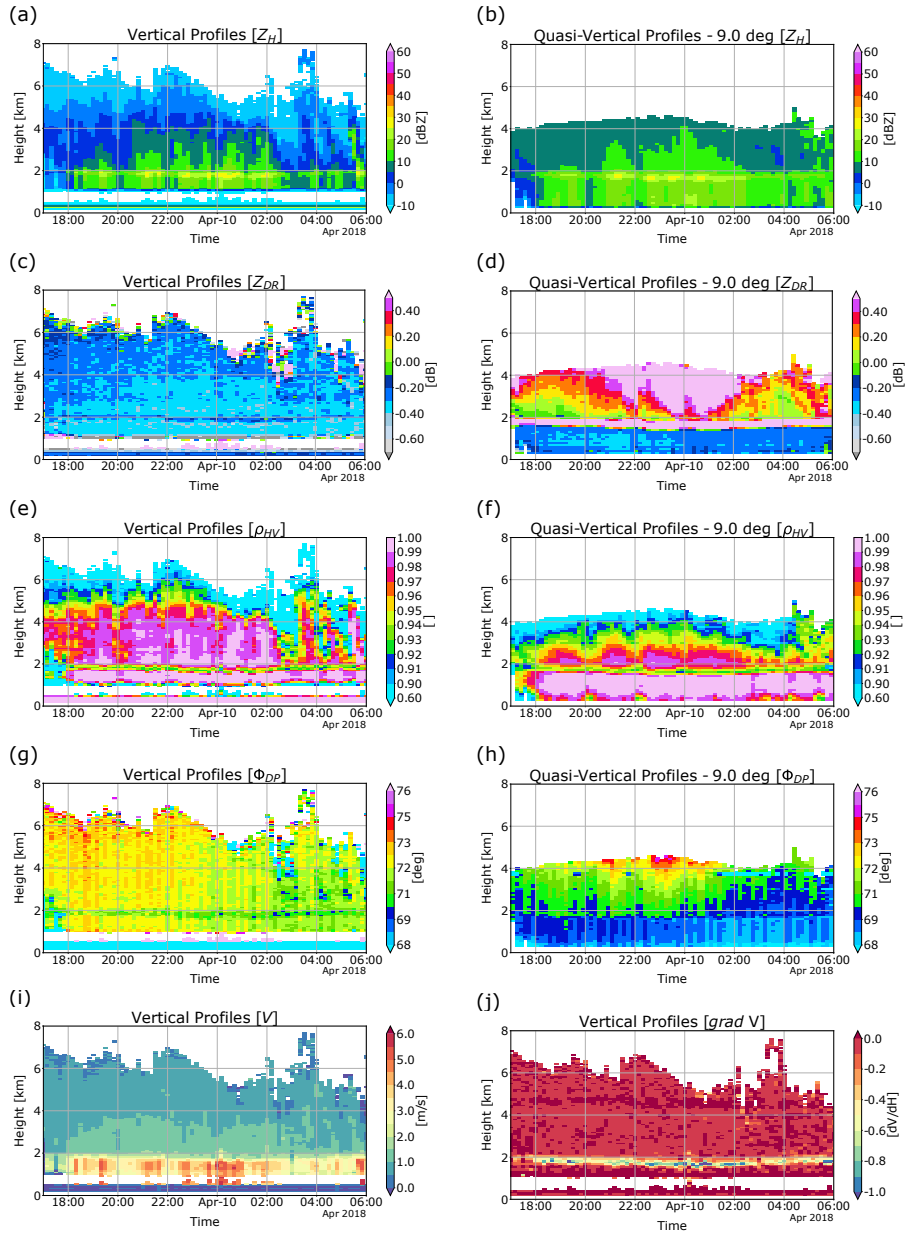
8

Figure 2. ~~HTI~~ Height-Time plots of Z_H (a-b), Z_{DR} (c-d), ρ_{HV} (e-f) and Φ_{DP} (g-h) generated from VPs (left) and QVPs (right) for a precipitation event recorded by a weather radar located at Chenies, UK. Also, (i) portrays the Doppler vertical velocity of hydrometeors, whilst (j) shows a plot of the profiles based on the gradient of V measurements ~~[dV/dh]~~ [dV/dH].

the upper boundaries of these enhancements ~~(i.e. the BB top) is related to the FL, just below 2 km in altitude. This enhancement is~~ to the ML. These enhancements are not necessarily at the same height in all polarimetric variables, but this has to do with
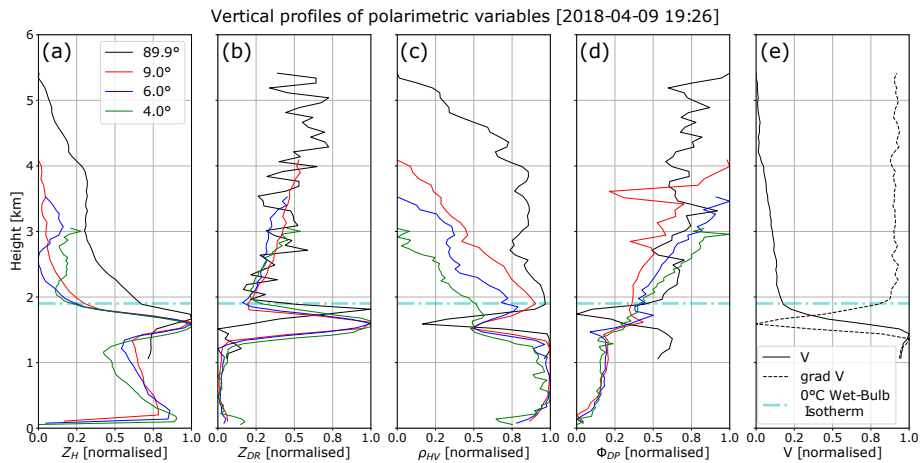
Figure 3. Normalised version of VPs and QVPs generated from polarimetric scans recorded at different elevation angles, related to a stratiform-type rain event. The $0°C$ wet-bulb height is shown with the dash-dotted line.

235   the backscattering properties of the melting particles and their relationship with the measured variable, as well as . Also, it is important to highlight that the methods used in the construction of the profiles , as demonstrated by Brandes and Ikeda (2004), Fabry and Zawadzki (1995) and Ryzhkov et al. (2016). Moreover, the QVPs provide the information below 1 km in elevation; this is important for the analysis of showers or events with freezing levels at relatively low altitudeplay a key role in the location of the peaks, i.e. both, VPs and QVPs result from an azimuthal averaging of the rays, representing an average structure of the

240   storm that helps to enhance the BB signature. So, the BB peaks in the VPs and QVPs in all radar measurements differ from the instantaneous profiles observed at individual slant ranges; this will be subject of discussion in Section 6.

     The reflectivity (Z_H) represents the power backscattered by precipitation particles, thus providing a general idea of information about the concentration, size , phase and water content and phase of the hydrometeors (Hong and Gourley, 2015). In Figures 2a and 2b demonstrates that , to a certain extent, it can be seen that the values of Z_H represent similar backscattered energy

245   taken either at vertical or horizontal elevations, this will be subject of analysis later on . It also can be seen on both , on both QVPs and VPs show similar intensities. Also, the well-known BB effect on Z_H , that yields a peak related to enhanced values of reflectivity due to the difference is visible on both profiles (around 1.7 km). The BB is caused by the increase in the dielectric factor for ice and water (Islam and Rico-Ramirez, 2014). As shown in Figure 3a, the constant of melting particles, by the change in size from large melting snowflakes to raindrops and by the increase in the fall speed of the hydrometeors

250   that reduce the particle concentration (Fabry, 2015). The BB is easily observed in stratiform events(close to 1.7 km); however, its boundaries do not always match the extents of the ML. Whilst for convective eventsit is difficult to set the melting layer boundaries based only on Z_H, e.g. in Figure 3a the top of the BB is not easy to discern. Moreover, the profiles of Z_H do not show a sharp BB feature , and thereforethe boundaries of the ML for this type of events are more challenging to identifythe BB feature in convective events; therefore, the estimation of ML for convective events based only on Z_H is not feasible.

255   The differential reflectivity (Z_{DR}) represents the difference between the ratio between horizontal and vertical reflectivity val-

ues (Z_H/Z_V) and it is related to the orientation, shape and size of the hydrometeors (Islam and Rico-Ramirez, 2014); therefore, Z_{DR} measurements for QVPs and VPs may describe different features of the particles as the elevation angle varies. For both QVPs and VPs, Z_{DR} profiles show similar behaviour in stratiform events: Figure 3b shows that Z_{DR} exhibit mean small slope changes on the rain medium (below 1.2 km), but there is a noticeable peak associated with the melting layer on both VPs and QVPs, and although there is a difference in the peak height between both formats, the top and bottom boundaries are at similar heights, especially for the QVPs. Brandes and Ikeda (2004) and Ryzhkov et al. (2016) showed that the presence of melting, randomly oriented ice particles within the melting layer and the mixing of hydrometeors produce the peaks in Z_{DR} often present in stratiform events. However, for profiles related to convective events (not shown), the VPs sometimes exhibit an inverse peak exactly above the rain medium and then generating a noisy, random pattern on the melting layer, that makes the estimation of the ML more difficult using VPs of Z_{DR}. Finally, the most significant difference for this variable can be seen in Figures 2c and 2d where the values of Z_{DR} for VPs and QVPs differ from each other, especially in the melting layer and above. It is also important to highlight that Z_{DR} provides valuable information for QPE. However, it usually shows a bias that must be corrected, e.g. in Figure 2c there is a bias in Z_{DR} (~ -0.35 dB) as we expect near-to-zero values for Z_{DR} in the rain region for vertically pointing measurements as raindrops are symmetrical on average when observed from underneath (Gorgucci et al., 1999). A subsequent analysis of 'birdbath' scans in light rain through the whole dataset confirmed a persistent offset in Z_{DR}. This reaffirms the importance of the detection of the melting layer boundaries, as it helps to set limits for the implementation of a Z_{DR} calibration algorithm.

The correlation coefficient (ρ_{HV}) measures the correlation between the backscatter amplitudes at vertical and horizontal polarisations. It is sensitive to the distribution of particle sizes and shapes, hence being sensitive to the hydrometeors phase, becoming a valuable hydrometeor classifier helping to identify non-meteorological echoes (Islam and Rico-Ramirez, 2014). Additionally, ρ_{HV} is a reliable indicator of the quality of the radar data as in the rain medium the correlation is close to 1, becoming an indicator of the quality of the polarimetric radar measurements (Kumjian, 2013a). Figures 2e and 2f show that ρ_{HV} is close to 1 within the rain region, this is a good indicator of the quality of the datasets. Figure 3c shows that the melting layer causes a similar response on ρ_{HV} as in Z_H and Z_{DR}, but in the opposite direction, resulting in a depression on the profiles starting at 1.4-1.5 km in height for QVPs and VPs, respectively. This depression results from the shift between high values of ρ_{HV}, related to raindrops and ice crystals and lower values triggered by the variety of shapes and axis ratios of the hydrometeors (Kumjian, 2013b). The behaviour of ρ_{HV} is similar on both, VPs and QVPs from $9°$ elevation, for stratiform or convective events, where the major difference lies in the depth of the depressions.

~~However, again, this~~ This may be caused by the resolution and elevation angle of the original scans~~(Ryzhkov et al., 2016)~~. On the other hand, the QVPs constructed from lower elevation angles, i.e. $4°$ and $6°$ exhibit less pronounced peaks related to the ~~ML~~ melting layer and a pronounced decrease ~~rate above 1.8 km that difficult the location of the FL. Additionally, ρ_{HV} is a reliable indicator of the quality of the radar data as Z_H, and Z_V are not equal, especially when measuring snow/ice or melting ice particles, however, in the rain medium their correlation is close to 1, becoming an indicator of the quality of the polarimetric radar measurements (Kumjian, 2013a) and then tends to decrease slightly for large oblate raindrops.Figures 2e and 2f show that ρ_{HV} is close to 1 within the rain region, this is a good indicator of the quality of the datasets.~~in ρ_{HV} above the BB that can make difficult to identify the ML.

As can be seen in Figures 2g, 2h, and 3d, the signatures of the ~~ML~~ melting layer on the differential propagation phase (Φ_{DP}) are, to a certain degree, ambiguous in our datasets, especially on the QVPs. Φ_{DP} ~~is a cumulative variable that~~ represents the difference ~~in phase between horizontal and vertical electromagnetic waves~~between the phase of the radar signal at horizontal polarisation and that at vertical polarisation, providing valuable information about the shape and concentration of the ~~particles~~ hydrometeors (Islam and Rico-Ramirez, 2014). Hence, the peaks on this type of profiles ~~are~~ may be related to a greater concentration of particles, ~~e.g. accumulation of melting or snowflake particles that may be related to the ML or the~~ due to the presence of the melting layer or the dendritic growth layer (DGL) as ~~demonstrated by Griffin et al. (2018)~~previously explored by Griffin et al. (2018), Kaltenboeck and Ryzhkov (2017) and Ryzhkov et al. (2016). Figure 3d shows that the QVPs of Φ_{DP} from $9°$ elevation, exhibit a small peak at 1.7 km in height related to the ~~backscatter differential phase~~melting layer, but is not as pronounced as with the other polarimetric variables, although there are significant peaks aloft (between 2.8 and 3.8 km), that may represent particle (ice or snowflakes) alignment on the DGL, as suggested by Kaltenboeck and Ryzhkov (2017), while lower elevation angles do not show strong signatures on the ~~ML~~ melting layer nor the DGL. In contrast, for $90°$ elevation scans, there is a well-defined depression in Φ_{DP} related to melting and particle growth (Brandes and Ikeda, 2004) at 1.8 km in height that closely matches the height of the BB; regarding the signatures of the DGL on the VPs, due to the noisiness of the profile above the ML, it is difficult to determine if these peaks are related to the DGL.

Last but not least, Figures 2i and 3e ~~shows~~ show the profiles related to the Doppler vertical velocities (V) and the signatures of the ~~ML~~ melting layer on this variable. It can be seen that the fall velocity [ms^{-1}] of the hydrometeors is relatively constant and close to zero above the ML, which is related to the fall velocity of ice and snow particles, then there is a sharp increase in the fall velocity of the precipitation particles in the melting layer ~~, and then~~ that becomes constant again in the rain region~~, having said that, it is difficult to incorporate this variable into an algorithm because their~~. However, it is challenging to incorporate the velocity profile into the ML detection because its features are not easy to identify ~~by~~ using an automated ~~procedure~~peak-search algorithm. Conversely, the VP of the gradient of V ($gradV$), shown ~~as the dotted line in Figure 3e~~in Figure 2j and in Figure 3e (dotted line), exhibits a ~~shape~~ BB enhancement and peak similar to the rest of polarimetric variables, where the upper and lower curvatures of the peak match ~~closely~~ the top and bottom extents of the ~~ML~~melting layer.

4 Algorithm to identify the ~~freezing~~ melting level

The melting level algorithm (MLA) has been designed to automatically detect the ML using either QVPs or VPs, under the premise that the peaks on each polarimetric profile and their curvatures are related to the melting layer. The MLA is based on the procedure proposed by Wolfensberger et al. (2016) that combines Z_H and ρ_{HV} to create a new profile with enhanced melting layer features. However, Figure 3 shows that there are additional variables, such as $[gradV]$, that may improve the identification of the ML. Therefore, we propose an algorithm that includes all the radar variables, computes all the possible combinations and estimate the melting layer boundaries. A subsequent analysis of the outputs of the algorithm in combination with radiosonde data determines the combination that is the best predictor of the ML. Some considerations are made for its design, e.g. to minimise the effect of beam broadening, the analysis is constrained to a height of 5 kilometres (for $9°$ scans, the height of the centre of the beam is similar to 30 km in range). Also, as shown in Figure 3, some profiles get noisy above the ML or contain spurious echoes aloft, making necessary to set an initial upper extent for the algorithm to work. The MLA is divided into two parts. The first part determines if the profile contains elements to detect the melting layer based on the combination of two profiles and setting an upper limit for its implementation. The second part estimates the ML based on a combination of the polarimetric profiles and their features. The algorithm uses either QVPs or VPs, but we avoid combining both profiles as VPs might not be available in other weather radar networks. A flowchart that illustrates the MLA steps is shown in Figure 4 and described below.

1. **Part 1**

   The first part of the MLA identifies profiles that are likely to contain signatures related to the melting layer and set an upper limit in the profiles to make use of all the available variables.

   1.a The algorithm takes advantage of the distinctive signatures on the profiles of Z_H and ρ_{HV} on both, VPs and QVPs, to perform an initial identification of rain echoes. These two profiles are normalised and combined into a single profile (P_{comb}) as suggested by Wolfensberger et al. (2016), but using different thresholds related to drizzle, heavy rain, snow and ice (Kumjian, 2013a; Fabry, 2015). Hence, values of Z_H between 5 and 60 dBZ and ρ_{HV} between 0.85 and 1 are normalised to 0 and 1: $[Z_H(dBZ)[5,60] \rightarrow Z_H^*[0,1]]$ and $[\rho_{HV}(\ )[0.85,1] \rightarrow \rho_{HV}^*[0,1]]$. Values outside these intervals are fixed to 0 and 1, correspondingly. The normalisation is carried out using the min-max normalisation procedure. Then, the normalised profiles are combined using the complement of ρ_{HV} to enhance the peaks present in the profiles:

   $$P_{comb} = Z_H^* \cdot (1 - \rho_{HV}^*) \tag{1}$$

   Note that (*) refers to a normalised variable.
   The profile P_{comb} is likely to show an enhanced peak if potential melting layer signatures were present in the profiles of Z_H and ρ_{HV}.
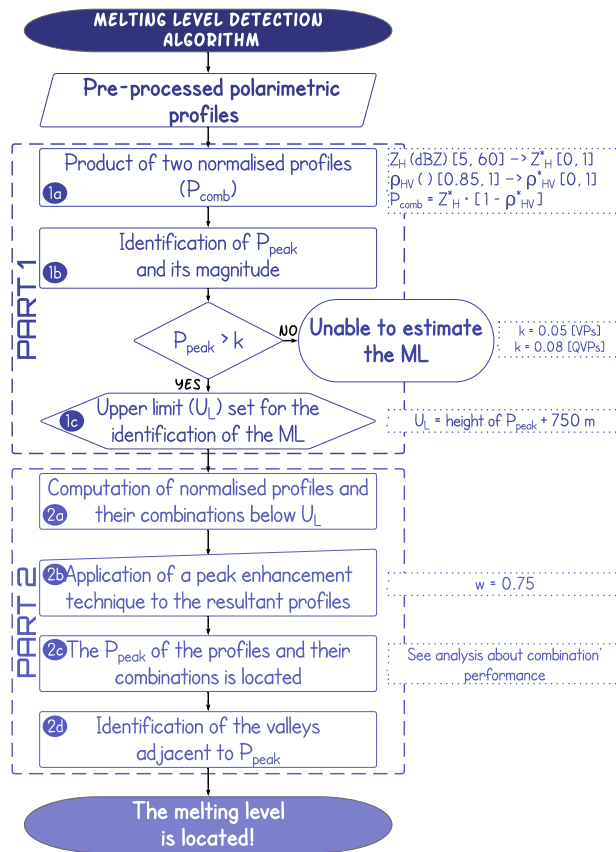
Figure 4. Flowchart of the proposed ~~FLA~~MLA.

1.b The ~~FLA~~ MLA locates the peaks on the profile P_{comb} comparing neighbouring values: a peak is a sample whose direct neighbours have smaller magnitudes. ~~Using this procedure, the inverse peaks~~Inversely, the valleys (or boundaries of the peaks) within the profile can ~~be defined as the valleys of P_{comb}; this enables the computation of the magnitude~~ ~~(k) of the peaks~~ also be detected using a similar rationale. As several peaks can be present in the profile, the peak with the higher magnitude (i.e. the horizontal distance between the peak and ~~its lowest valley. The peak with the~~ ~~higher magnitude~~ the origin) is set as P_{peak}. ~~If the magnitude (k)~~ Then, to identify profiles with a P_{peak} strong enough to be related to potential melting layer signatures, a threshold 'k' is set: if the magnitude of P_{peak} is less than ~~the threshold k,~~ (set to 0.05 for VPs ~~or~~ and 0.08 for QVPs~~, the FLA~~), the MLA determines that the gradients are not strong enough to correspond to ~~ML~~ melting layer signatures and therefore the profile does not contain elements to detect the ~~FL.~~ ML. This step is illustrated in Figure 5a, where the magnitude of P_{peak} (~ 0.14) is greater than the threshold 'k'. Further discussion on the ~~values of these parameters~~ value of this parameter is provided in ~~the next sections.~~ Sections 4.1 and 6.

14

1.c ~~Otherwise~~If the magnitude of P_{peak} is greater than k, an upper limit (U_L) is set taking the height of P_{peak} and adding 750 meters above. This value is selected ~~to locate the top of the ML from the ML peak. Usually the ML thickness (i.e. between BB bottom and BB top)~~ as usually, the melting layer thickness can reach values less than about 800 m (Fabry and Zawadzki, 1995)~~,~~; hence 750 m is sufficient to ~~locate the top~~ refine the search of the ML. Figure 5a illustrates ~~the first stepof the algorithm~~this step, where 750 m are added to the height of P_{peak} (~ 1.51 km) to set an upper limit (~ 2.26km).

2. **Part 2**

   ~~Once U_L is defined, the algorithm identifies the $0°C$ height based on a profile that is the result of the combination of several polarimetric profiles as follows~~In the second part of the algorithm, we incorporate the rest of the polarimetric variables to analyse its capabilities to refine the detection the melting layer boundaries and determine the combination that better detects the ML.

   2.a ~~The profiles of the available polarimetric variables have an upper limit set by~~ In this step, the profiles of all the radar variables are cut below U_L~~to search for the FL. Every individual profile is normalised. Note~~. Then, and considering that Z_H^* and ρ_{HV}^* were already normalised in step 1.a, ~~whereas the rest of the variables are normalised~~ the other variables are also normalised but using the minimum and maximum values ~~of each variable. A new profile is computed following Equation 2 for VPs or Equation 3 for QVPs:~~ in each profile as thresholds. To incorporate all the variables into the algorithm, the complement of the variables is used when appropriate. This is made to generate profiles with analogue peaks that enhance the footprints of the melting layer when combined with other variables. Equation 2 and Equation 3 are derived based on the patterns observed in VPs and QVPs. These equations vary according to the combination of the variables presented in Table 2.

   $$P_i^* = (1 - gradV^*) \cdot (Z_H^*) \cdot (Z_{DR}^*)$$
   $$\cdot (1 - \rho_{HV}^*) \cdot (1 - \Phi_{DP}^*) \quad (2)$$

   $$P_i^* = (Z_H^*) \cdot (Z_{DR}^*) \cdot (1 - \rho_{HV}^*) \cdot (\Phi_{DP}^*) \quad (3)$$

   where i ~~depends on the combination of the variables used according to Table 2.~~

   2.b ~~P_i^* will very likely show a peak within the ML. To refine the boundaries of this peak i.e. the valleys adjacent to the peak, the FLA applies a peak-enhancement technique expressed by:~~

   $$P_i = P_i^* - (w \cdot P_i^{*\prime\prime})$$

   ~~Where P_i is the enhanced profile, P_i^* is the profile given by Equations 2 or 3, w is a weighting factor and $P_i^{*\prime\prime}$ is the second derivative of P_i^*. The optimum choice of the parameter w depends upon the signal-to-noise ratio and the desirable sharpening extent. Table 2 lists the enhanced profiles produced by combining different polarimetric~~

~~profiles, and Figure 5b shows the enhancement of the peak and valleys. Details on the choice of the parameter w are presented in the following sections.~~

~~2.c For each profile P_i, the magnitude (k) of P_{peak} is computed as in step 1.b. The same threshold $k < 0.05$ for VPs ; $k < 0.08$ for QVPsis applied in this step.~~

~~2.d Figure 5b shows that the valleys of the profile P_i are related to the boundaries of the ML. These valleys can be placed by searching the inverse peaks directly above and below P_{peak}. Finally, the algorithm allocates the top valley of P_i as the estimated height of the FL (FL_e).~~

depends on the combination of the variables used according to Table 2.

Table 2. Possible combinations of polarimetric variables for VPs and QVPs used ~~on~~ for the ~~FL estimation~~ML detection.

[VPs]	[QVPs]	P_1	P_2	P_3	P_4	P_5	P_6	P_7	P_8	P_9	P_{10}	P_{11}	P_{12}	P_{13}	P_{14}	P_{15}
$1-gradV^*$	-	○	○	○	○	○	○	○	○	○	○	○	○	○	○	○
Z_H^*	Z_H^*	○	○	○	○	○	○	○	●	●	●	●	●	●	●	●
Z_{DR}^*	Z_{DR}^*	○	○	○	●	●	●	●	○	○	○	○	●	●	●	●
$1-\rho_{HV}^*$	$1-\rho_{HV}^*$	○	●	●	○	○	●	●	○	○	●	●	○	○	●	●
$1-\Phi_{DP}^*$	Φ_{DP}^*	●	○	●	○	●	○	●	○	●	○	●	○	●	○	●

[VPs]	[QVPs]	P_{16}	P_{17}	P_{18}	P_{19}	P_{20}	P_{21}	P_{22}	P_{23}	P_{24}	P_{25}	P_{26}	P_{27}	P_{28}	P_{29}	P_{30}	P_{31}
$1-gradV^*$	-	●	●	●	●	●	●	●	●	●	●	●	●	●	●	●	●
Z_H^*	-	○	○	○	○	○	○	○	○	●	●	●	●	●	●	●	●
Z_{DR}^*	-	○	○	○	○	●	●	●	●	○	○	○	○	●	●	●	●
$1-\rho_{HV}^*$	-	○	○	●	●	○	○	●	●	○	○	●	●	○	○	●	●
$1-\Phi_{DP}^*$	-	○	●	○	●	○	●	○	●	○	●	○	●	○	●	○	●

Note: * refers to the normalised version of the variables.

The algorithm computes all the possible combinations of the profiles to analyse the influence of each variable, in this case, generating 31 different profiles if using VPs and 15 profiles when using QVPs.

2.b The profiles (P_i^*) generated in the previous step will very likely show a peak related to the melting layer. The next step in the MLA is to apply a peak-enhancement technique to refine the boundaries of this peak. This can be done using the following equation:

$$P_i = P_i^* - (w \cdot P_i^{*''}) \tag{4}$$

Where P_i is the enhanced profile, P_i^* is the profile given by Equations 2 or 3, w is a weighting factor and $P_i^{*''}$ is the second derivative of P_i^*. The optimum choice of the parameter w depends upon the signal-to-noise ratio and the desirable sharpening extent. Table 2 lists the enhanced profiles produced by combining different polarimetric

profiles, and Figure 5b shows the enhancement of the peak and valleys. Details on the value of the parameter w are presented in the Sections 4.1 and 6.

2.c For each profile P_i, the maximum enhancement in the BB has a magnitude given by P_{peak} and computed as in step 1.b. Then the parameter k is used to discard profiles with peaks not related to the melting layer [$k = 0.05$ for VPs; $k = 0.08$ for QVPs].

2.d The top and bottom boundaries of the BB enhancement in P_i can be placed by searching the inverse peaks (valleys) directly above and below P_{peak}. Finally, the algorithm allocates these points as the boundaries of the melting layer. This step is shown in Figure 5c, where the selected profile P_{26} is highlighted. The top valley of P_i is set as the estimated height of the ML (ML_{Top}).
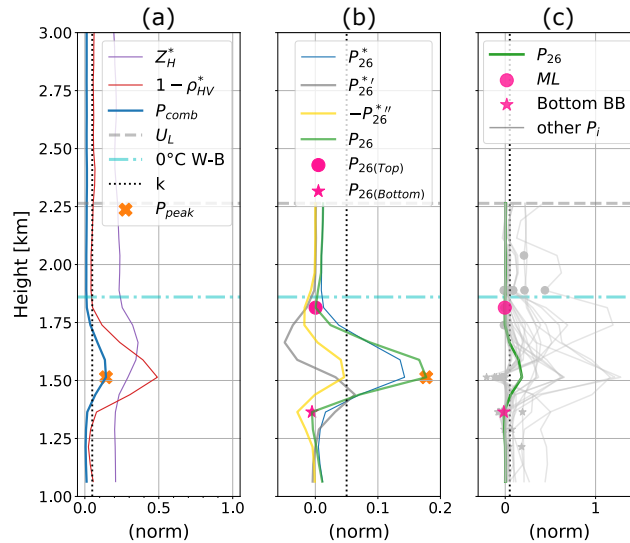

Figure 5. Depiction of the implementation of the algorithm for the ~~FL estimation~~ML detection.

As can be seen in Figure 5a, the combination of Z_H^* and $1 - \rho_{HV}^*$ produces a profile with a peak (P_{peak}) ~~related to the ML~~ that is useful to ~~estimate the FL. The magnitude (k) of P_{peak}~~ detect the presence of the melting layer. An adequate choice of the magnitude of the parameter (k) is important to discard profiles ~~that do not have a strong enhancement~~ with a P_{peak} that is not strong enough to be related to the ~~ML~~melting layer. However, additional variables can be used (see Equations 2 and 3) to refine the ~~estimation of the FL~~ detection of the ML. The upper limit (U_L) allows the use of other variables that otherwise could not be part of the algorithm due to noisiness or spurious echoes present at the top of the profiles. Figure 5b shows the importance of the refinement of the profile, e.g. the profile combination $P_{26}^* = (1 - gradV^*) \cdot (Z_H^*) \cdot (1 - \rho_{HV}^*)$ (blue line) has a peak related to the ~~ML~~melting layer and the valley located at the top of this peak is close to the ~~FL~~ML, but it is difficult for a peak-detection algorithm to detect its height as it is not as pronounced as required. The use of the first derivative of the profile, i.e. ~~P_{26}'~~$P_{26}^{*'}$ (grey line), is not helpful as the peaks are not close to the ~~FL~~ML. The profile P_{26} (green line) results from the

implementation of Equation 4, where a value of $w = 0.75$ enhance the peak and its valleys enough for the algorithm to detect their location. A proper choice of the parameter w depends on the desired weight to the original profile rather than its second

440 derivative. The impact of the parameters k and w ~~into the algorithm will be~~ on the algorithm is discussed in the following ~~sections~~section.

5 ~~Results~~

4.1 ~~VP and QVP comparison~~Implementation of the ML algorithm

~~To support the performance and outputs of the algorithm is necessary to assess the consistency between the available radar~~
445 ~~data. Given that the polarimetric variables portray the echoes depending on the elevation angle where they were taken, it is~~
~~only possible to compare QVPs and VPs of Z_H, as these variables measure similar properties of the raindrops taken either~~
~~at low-elevation angles ($4°$, $6°$ and $9°$) or 90-deg elevations respectively. From the total of 94 rainfall events, we carried out~~
~~a manual classification of rain events according to the findings of Fabry and Zawadzki (1995) and Rico-Ramirez et al. (2007)~~
~~. A total of 68 events were classified as stratiform. This category includes low-level rain and rain with BB as they showed the~~
450 ~~well-known enhancement of reflectivity observed within the ML or look-alike drizzle events below the $0°C$. On the other hand,~~
~~26 events recorded mainly during the summer met the characteristics of showers, i.e. indistinguishable signatures of the ML~~
~~in the Z_H profiles, in which higher values of reflectivity are present; the latter is the type of precipitation that is less common~~
~~in the UK (Collier, 2003). The comparison between VPs and QVPs takes into account the time stamp and spatial resolution of~~
~~the profiles. The Pearson correlation coefficient (r) is computed to analyse the consistency between the VPs and QVPs. The~~
455 ~~results for stratiform and convective events are shown in Figures 6 and 7, respectively.~~
~~Comparison of VPs and QVPs of Z_H generated at three elevation angles for a collection of stratiform events. Counts indicate the number of points in the hexagon~~
~~As in Fig. 6, but for a collection of convective events. Counts indicate the number of points in the hexagon~~
~~Figure 6a shows that the agreement between VPs and QVPs (constructed from $9°$ scans) resides on relative low values of~~
460 ~~reflectivity, that are most probably related to light and moderate rain rates; this is expected for stratiform-type events. Figures~~
~~6b and 6c show that the agreement diminishes when decreasing the elevation angle, whilst higher values of Z_H do not always~~
~~find their pairs as the elevation decrease. This could be explained by the averaging process carried out in the construction~~
~~process of the profiles, as the radar resolution volume increases with distance. On the other hand, Figure 7 shows a more~~
~~scattered distribution of Z_H for shower-type events. Higher values of Z_H, related to moderate to heavy rain-rates are present.~~
465 ~~Again, the correlation decreases for lower elevation angles, and it can be seen that there are mismatches for cells with higher~~
~~values of reflectivity.It is worth mentioning that a similar analysis was carried out using other polarimetric variables, but as~~
~~expected, the results were not consistent as only Z_H describe similar properties of the precipitation measurements taken either~~
~~at horizontal or vertical elevation angles.~~

4.2 ~~Implementation of the FL algorithm~~

470 ~~As described in section ??, the FLA~~ As described before, the MLA performs a pre-classification of profiles ~~that are~~ likely to contain ~~signatures related to the ML~~ melting layer signatures. Some tests were carried out by replacing Z_H^* with other variables (e.g. Z_{DR} or $1 - gradV^*$) to ~~see if there is any improvement~~ identify improvements in the pre-classification. From Figure 3b it is clear that the QVPs of Z_{DR} exhibit a pronounced peak related to the ~~ML~~ melting layer even for low elevation angles, but unfortunately Z_{DR} is not calibrated and the thresholds for normalising this variable may vary depending on the elevation angle.

475 On the other hand, replacing Z_H^* with the profile $1 - gradV^*$ for the VPs could improve the pre-classification, but this may restrict the implementation of the algorithm, i.e. it would be only applicable if vertical velocity profiles are available. Although we observed some improvements using these variables in the first part of the ~~FLA~~ MLA, especially for ~~convective events~~ rain showers, we wanted to keep this part as simple and robust as possible to ~~avoid a complex~~ enable the reproducibility of the algorithm. Hence we used the combination of Z_H^* and ρ_{HV} for part 1 of the algorithm as initially proposed by Wolfensberger

480 et al. (2016).

~~Also, as shown in Figures 4, 5a, 5b and Equation 4,~~ On the other hand, the algorithm relies on the parameters k and w, as shown in Figures 5a, and 5b. These parameters can be adjusted according to the radar datasets, e.g. the parameter k can be affected by the quality of ρ_{HV}: in our datasets and after the removal of non-meteorological echoes, ρ_{HV} exhibits values close to 0.85 in the ~~ML~~ melting layer, on both QVPs and VPs, but this may vary depending on the type of radar, scanning strategy and quality

485 of the datasets. We set $k = 0.05$ for VPs and $k = 0.08$ for QVPs empirically, and these values allow the algorithm to discard enhancements in the profile not ~~strong enough to be~~ related to the ~~ML.~~ melting layer. Moreover, several tests were carried out using time-averaged QVPs, resulting in smoother profiles, and this parameter was helpful to identify profiles with melting layer signatures. On the other hand, Equation 4 is applied to the profiles to enhance the ~~peaks (and~~ BB peak and the top/bottom boundaries (i.e. valleys) within the profile, thus refining the detection of the ~~FL~~ ML. This equation combines the original profile

490 with its second derivative, ~~that can be~~ weighted with the parameter w. As shown in Figure 5b, the second derivative of the profile (yellow line) exhibits deeper peaks, but its top boundary is still far from the measured ~~FL~~ ML. After several trials, we set $w = 0.75$ as this value proves to enhance the peaks of the original profile without compromising the match of the top boundary and ~~hence, improving the estimation of the FL. Again~~ improving the ML detection. Likewise, this parameter can be adjusted depending on the radar datasets, e.g. profiles that exhibit smoother peaks due to the nature of its construction process and the

495 resolution of the original scans, or profiles with vertical resolution too coarse can be adjusted with the parameter w for a better ~~performance of the algorithm.~~ algorithm performance.

4.2 ~~FL estimation from VPs~~

~~The performance of the FL estimation from VPs is compared against the FL measured by radiosonde data~~

19

5 Results

5.1 VP and QVP comparison

Both VPs and QVPs proved to be an efficient way to monitor the temporal evolution of the melting layer, but the elevation angle used to build the QVPs affects in different ways each radar variable, as described in Section 3 and shown in Figures 2 and 3. Hence, to support the performance and outputs of the algorithm, we assessed the consistency between the Z_H profiles constructed from different elevation angles, as this is the variable less prone to significant variations due to the elevation angle. For the rest of the variables, it is not possible to compare QVPs as their characteristics vary with the elevation angle used to build the QVPs.

To carry out this analysis, we manually classified the rain events recorded by the radar according to the recommendations of Fabry and Zawadzki (1995) and Rico-Ramirez et al. (2007). From the total of 94 rainfall events, 68 events were classified as stratiform. This category includes low-level rain and rain with BB as they showed the well-known enhancement of reflectivity observed within the melting layer or look-alike drizzle events below the $0°C$. On the other hand, 26 events recorded mainly during the summer met the characteristics of showers, i.e. indistinguishable signatures of the melting layer in the Z_H profiles, in which higher values of reflectivity are present; the latter is the type of precipitation less common in the UK (Collier, 2003). The comparison between VPs and QVPs takes into account the time stamp and spatial resolution of the profiles. The Pearson correlation coefficient (r) is computed to analyse the consistency between the VPs and QVPs. The results for stratiform and convective events are shown in Figures 6 and 7, respectively.

Figure 6 shows that reflectivity values related to light and moderate rain rates (expected on stratiform-type events) are similarly depicted on both VPs and QVPs. However, the agreement diminishes when decreasing the elevation angle, mainly because higher values of Z_H do not always match their pairs as the elevation decrease. This could be explained by the averaging process carried out in the construction process of the profiles, as the radar resolution volume increases with distance. On the other hand, Figure 7 shows a more scattered distribution of Z_H for shower-type events, in which higher values of Z_H (related to moderate to heavy rain-rates) are present. Again, the correlation decreases for lower elevation angles, and it can be seen that there are mismatches for cells with higher values of reflectivity. This can be related to local storm effects and spatially nonuniform convective elements present in the QVPs, as explored by Ryzhkov et al. (2016). It is worth mentioning that QVPs constructed from lower elevation angles were also assessed (results not shown), but similar behaviour was observed, e.g. correlation decreases even further. Also, a similar analysis was carried out using other polarimetric variables. However, the results were not consistent as only Z_H describe similar properties of the precipitation measurements taken at these elevation angles.

5.2 ML detection from VPs

The MLA outputs were analysed to find the combination of VPs that better detects the ML. These outputs are compared against $0°C$ wet-bulb isotherms over one year of rainfall events. Since soundings are released twice daily, the radiosonde data is extended at several time-steps to create short time-windows and enable a comprehensive comparison with the radar data.
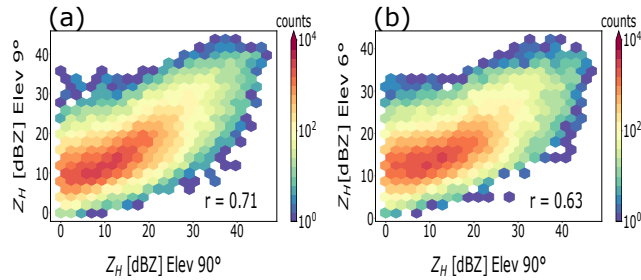
Figure 6. Comparison of VPs and QVPs of Z_H generated at two elevation angles for a collection of stratiform events. Counts indicate the number of points in the hexagon
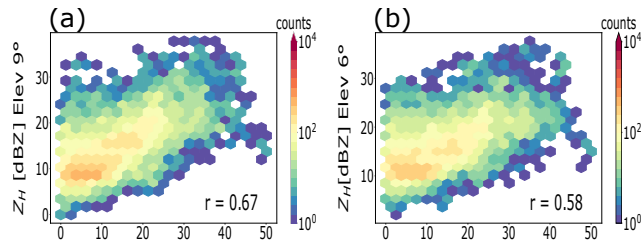

Figure 7. As in Fig. 6, but for a collection of convective events. Counts indicate the number of points in the hexagon

Performance metrics [Pearson correlation coefficient (r), Mean Absolute Error (MAE), Root Mean Square Error ($RMSE$)] between the ~~measured (FL_{RS}) and estimated (FL_e) FL heights~~ height of the $0°C$ Wet-Bulb isotherm and the estimated ML are computed. Figure 8 shows the results for a 60-min window, i.e. the ~~measured (FL_{RS}) is set as constant for~~ height of the $0°C$ Wet-Bulb isotherm is assumed constant 30-min before and after the time stamp of the radiosonde.

Figure 8 shows the ~~influence~~ capabilities of all polarimetric variables ~~on the estimation of the FL~~ for the detection of the ML. In Figure 8a, the variable *n profiles* is an indicator of the ~~additional false-positive cases that can be detected by each combination, this takes place due to the presence of peaks not related to the ML but~~ number of profiles that, according to the algorithm, contain peaks strong enough to ~~surpass by the first part~~ be related to the melting layer. This variable can only be validated by a visual inspection of the algorithm ~~, e.g. profiles that contain only one variable or combinations that engage Φ_{DP} into the analysis, where strong peaks are found but not associated with the ML~~ outputs, as some variables may incorrectly classify some peaks as melting-layer-related. Overall, Figure 8 shows that the combinations that include Z_H^*, $[1 - \rho_{HV}^*]$ or $[1 - gradV^*]$ improve the accuracy of the ~~FLA~~ MLA e.g. P_9, P_{11} or P_{26}, as the correlation and the errors are relatively low for these combinations. After a visual assessment of the performance of each ~~profile and in combination with~~ combination and supported by the statistics computed above, we determine that the profile combination $P_{26} = [Z_H^* \cdot (1 - \rho_{HV}^*) \cdot (1 - gradV^*)]$ ~~shows better performance for the estimation of the freezing level. We magnified the time window~~ is the best predictor of the ML. Then, several time windows are set to assess the ~~variation of the FL and the~~ accuracy of the ~~FLA using the profile P_{26}~~ MLA over one year of radar data. ~~This is~~, as shown in Figure 9. ~~Figure 9~~ This analysis confirms the good performance of
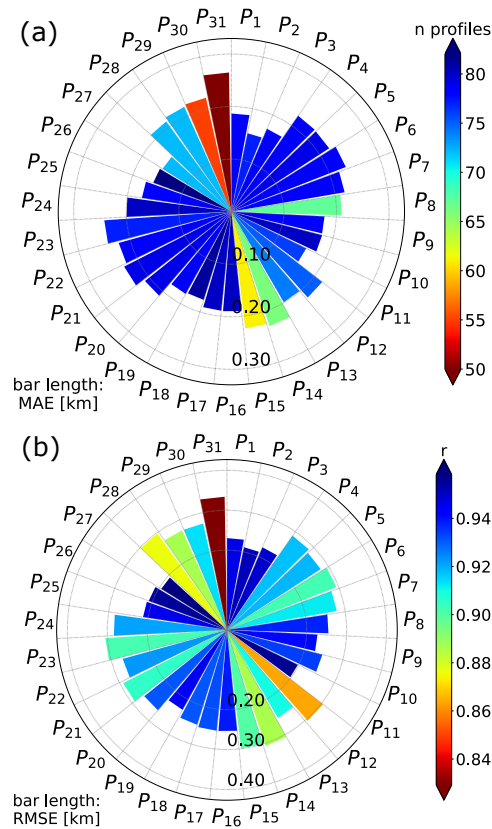
Figure 8. Errors in the ~~FL estimation~~ ML detection for VP using a ±30 minute window. In (a) the bar length represents the MAE (in km) ~~for every polarimetric combination~~ and colour represents the number of vertical profiles ~~analysed for~~ with strong signatures detected by every polarimetric combination; in (b) the bar length represents the RMSE (in km) for every polarimetric combination and colour represents ~~r.~~ the Pearson correlation coefficient

the combination P_{26} on the ~~FL estimation~~ ML detection, even when increasing the time window, ~~with errors~~ as the $RMSE$

550   and MAE are close to 200 m and ~~high correlation coefficients. As expected, the larger the time window, the larger the errors, as the number of profiles included in the analysis increases and~~ $r = 0.95$. Another indicator taken into account in the visual inspection of the algorithm output was the detection of the ~~measured FL is likely to vary during this period~~ melting layer bottom and its steadiness regarding the ML.

      Examples of the ~~estimation of the FL on~~ detection of the melting layer for stratiform and convective events ~~for profiles~~ using

555   the profile P_{26} ~~and P_{16}~~ are shown in Figure 10. Figures ~~13a and 13b, displayed over an HTI plot of reflectivity , show that running the algorithm using the~~ 10a and 10b, show HTI plots of reflectivity and velocity gradients and the output of the MLA using combination P_{26} in both, stratiform or convective events ~~, yields~~. The algorithm shows a good performance ~~of the FL estimation~~, especially for stratiform events ~~, where the FL~~ where the ML height and the rain zone ~~is~~ are accurately defined. For the convective event, the ~~FL~~ ML is correctly identified, albeit the bottom of the ~~ML is not~~ melting layer is not entirely
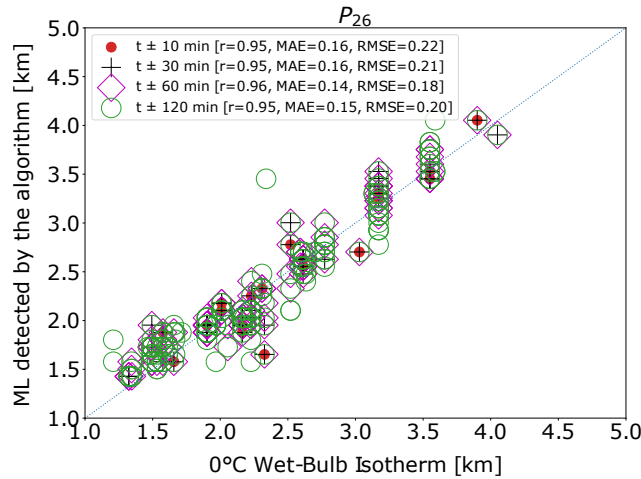
22

Figure 9. Heights of the $0°C$ ~~wet-bulb~~ isotherm ~~measured by radiosonde~~ versus ~~FL estimated~~ ML detected by the algorithm using the combination P_{26} for several time windows. The 1:1 line is shown in blue. MAE and RMSE in km.

560   detected. This ~~highlights the problem of the algorithm when describing low-altitude melting layers~~ is a drawback when using the algorithm based on VPs ~~. Similarly, Figures 10c and 10d, displayed over an HTI plot of velocity gradients, exemplify the performance of the algorithm based on the profile P_{16} where the variable $[1 - gradV^*]$ confirms its capacity to detect the FL~~and highlights the problems when low-altitude melting layers are present.

5.3   ~~FL estimation~~ ML detection from QVP

565   ~~The FLA is applied to~~ The MLA is applied using QVPs generated from scans at three different elevation angles ($4°$, $6°$ and $9°$). After several trials on the parameters k and w ~~of the algorithm~~ in the algorithm implementation, only the highest elevation produced satisfactory ~~results on the FL estimation~~ ML estimation results. The explanation of this has its foundation in Figure 3c, where QVPs from lower elevation angles display shapes that ~~make~~ complicate the implementation of the algorithm~~difficult~~. For instance, the profile of ρ_{HV} exhibits a peak related to the ML, but above this peak the values of ρ_{HV} decrease sharply,

570   whilst the profile of Z_H exhibits smoother peaks and when the normalisation process is carried out, the parameter k ~~is not able to identify gradients strong enough to be~~ cannot correctly filter gradients related to the ML. Thus, after several trials and supported by the analysis presented in Section ~~??~~5.1, we decided not to use the lower elevation angles ($4°$ and $6°$). Using the same windows as in the ~~vertical profiles~~VPs, we computed several performance metrics ($r, MAE, RMSE$) between the $0°C$ ~~isotherms measured by the radiosondes and the estimated by the FLA~~wet-bulb isotherms and detected MLs. The performance

575   of the algorithm using different profiles and a time window of 60-min (i.e. using radar profiles 30-min before and after the radiosonde timestamp) is shown in Figure 11.

     Figure 11a shows that the number of profiles covered by the time window is somewhat ~~more significant~~ greater than the number of profiles covered in the implementation of the VPs. This is expected ~~given that~~ because the coverage area of the PPIs
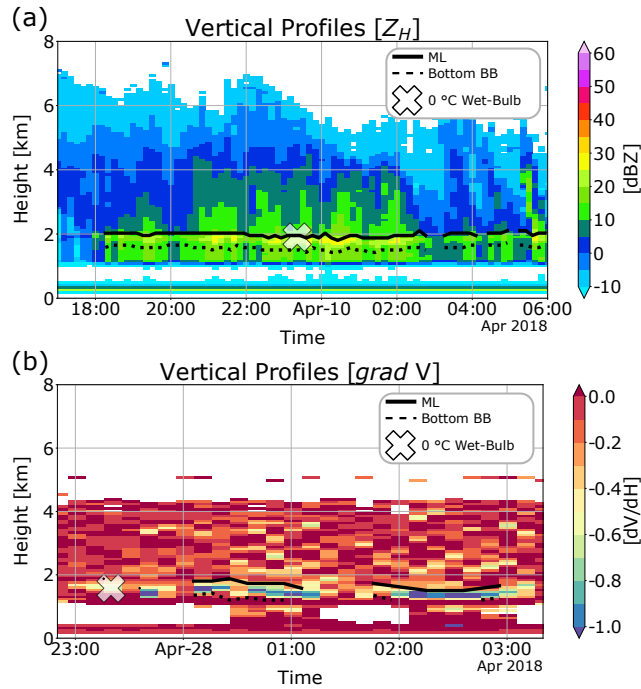
Figure 10. Comparison of the ~~FLA~~ MLA outputs based on the variable P_{26} at 90° elevation angle ~~using~~ for two different ~~variables~~ rain events: (a) ~~and (b) show~~ shows the ~~performance~~ detection of the ~~variable P_{26}~~ melting layer for a stratiform ~~(top left) and a convective~~ event ~~(top right); (c)~~ displayed over an HTI plot of Z_H, and (~~d~~b) ~~display~~ shows the performance ~~of the variable P_{16}~~ for a ~~stratiform (bottom left) and a~~ convective event ~~(bottom right)~~ displayed over an HTI plot of $gradV$.

from where the QVPs were constructed is greater ~~compared to~~ than the vertical scans. Overall, the four indicators in Figure 11
580 stress the influence of Z_H and ρ_{HV} in the estimation of the ~~FL~~ ML height and reveal that ~~appending~~ adding the combination Z_{DR}^* to the analysis, i.e. P_{12}, P_{14} or P_{15} improve the delimitation of the ML, given that these combinations exhibit high values of correlation ~~((r))~~ (r) and the errors are below ~~300~~ 250 m. Based on these results, and combined with a visual assessment of the outputs of the algorithm over a whole year of precipitation profiles, we concluded that the profile that combines Z_H^*, Z_{DR}^* and $(1 - \rho_{HV}^*)$, i.e. P_{14} provides ~~a better estimation of the freezing level~~ the best detection of the ML. The performance of the
585 algorithm using this combination is shown in Figure 12.

Figure 12 shows that error and correlation coefficient decrease as the time-interval increase. Given that the errors are close to 250 m for short-time windows, this combination proves to be accurate for the ~~FL estimation~~ ML detection, making allowance for the original resolution of the scans (600 m). Two examples of the outputs of the algorithm ~~selecting the combinations P_{10} and~~ using the profile P_{14} ~~as the final product~~ are shown in Figure 13 for the same stratiform and convective events as in
590 section ~~??. Figures 13a and 13b show the outputs of the algorithm using the combination P_{10}, displayed on a base-HTI plot of Z_H, where the performance for a stratiform event is acceptable, given the presence of random, noticeable peaks along to the duration of the event, whereas the performance of this combination for the shower event is less accurate, due to the absence~~
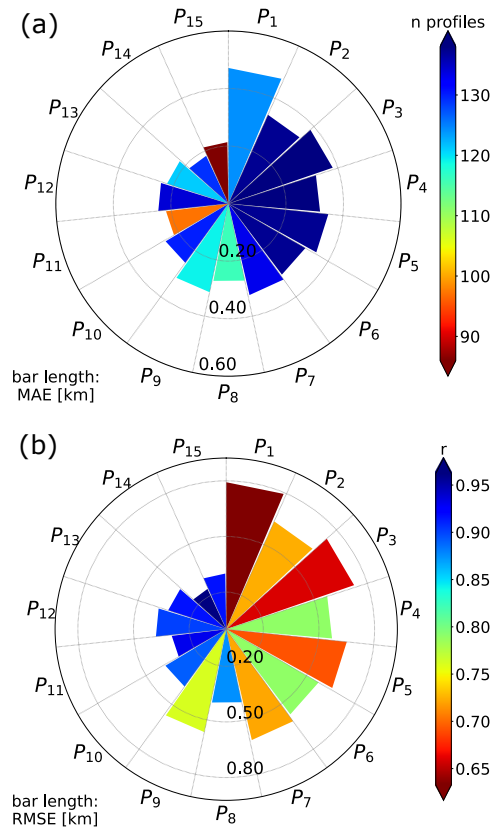
24

Figure 11. Errors in the ~~FL estimation~~ <u>ML detection</u> for QVPs using a ± 30 minute window. In (a) the bar length represents the MAE (in km) ~~for every polarimetric combination~~ and colour represents the number of QVPs ~~analysed for~~ <u>with strong signatures detected by</u> every polarimetric combination; in (b) the bar length represents the RMSE (in km) <u>for every polarimetric combination</u> and colour represents ~~r.~~<u>the Pearson correlation coefficient;</u>

~~of strong gradients on the profile computed in the first part of the algorithm and emphasised on the second one. On the other hand, the combination~~ <u>5.2. The combination</u> P_{14} ~~, displayed on a base-HTI plot of~~ Z_{DR}~~, shows better performance, especially for the stratiform event shown in Figure 13c, as the FL is precisely~~ <u>shows that the ML is correctly</u> detected and the delineation of the rain region is well-executed. For the convective event of Figure 13~~c~~<u>b</u>, the outputs of the algorithm are accurate for the ~~FL~~ <u>ML</u> estimation although some gaps are present due to the filtering of profiles in the first part of the algorithm.

6 Discussion

We constructed VPs and QVPs of polarimetric variables to explore precipitation events and its features. As shown in Figure 2, both types of profiles display differences that are influenced by the scan elevation angle and the methods used for the construction of the profiles (Giangrande et al., 2008; Kumjian and Lombardo, 2017; Ryzhkov et al., 2016). <u>Regarding the construction</u>
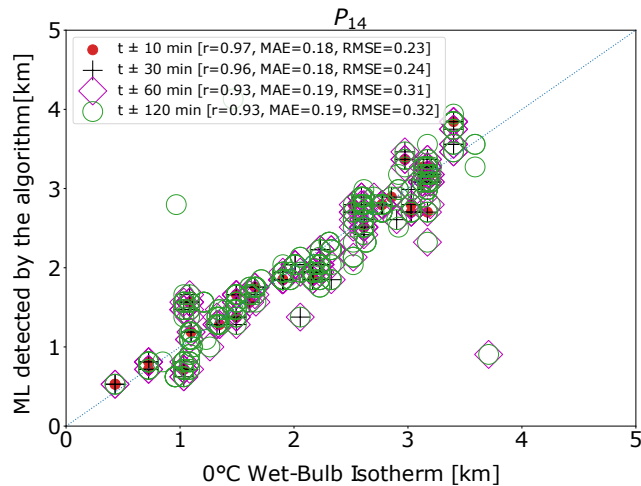
Figure 12. Heights of the $0°C$ ~~wet-bulb~~ isotherm ~~measured by radiosonde~~ versus ~~FL~~ ML estimated by the algorithm for several time windows using QVPs from $9°$ elevation scans. The 1:1 line is shown in blue. MAE and RMSE in km.

process of the profiles, there are several points worth discussion: (i) it is possible to generate 'time-averaged' QVPs to smooth the effects related to local storm structures, as the averaging process over the radar domain combined with temporal averaging may reduce the signal noise and, at some extent, it is possible to discard profiles with signatures not related to the melting
605 layer. However, the duration of the rain events and other factors raise a question about the correct time-window length. After several attempts with different time-windows, we observed that for stratiform events, the signatures of the melting layer are often easier to discern, but for convective events, variables that may help to detect the ML, e.g. Z_{DR} or ρ_{HV}, are affected by the temporal averaging, blurring the melting layer signatures. Thus, we present examples of 'instantaneous' QVPs; however, we kept in mind this matter for the MLA design; (ii) the spatial variation of the rain events is a limitation of both, VPs and QVPs.
610 The former capture the storm structure only directly above the radar location; on the other hand, for the QVPs the PPIs may contain sectors with non-homogeneous echoes, e.g. at distant ranges from the radar where the beam is considerably bigger, combining mixed precipitation or at earlier stages of the storm evolution, where such echoes are not sufficient to generate QVPs with clear signatures of the melting layer or even valid QVPs. This horizontal heterogeneity introduces uncertainty into the QVPs, as stated by Ryzhkov et al. (2016). This limitation on the generation of the QVPs requires further investigation and
615 it is out of the scope of this work, being our main objective the detection of melting layer signatures; (iii) due to the averaging process on the construction of the profiles, the BB shape and the height of the BB peak do not exactly match profiles found in previous studies, especially from profiles generated from measurements collected using vertical cross-sections. For instance, Brandes and Ikeda (2004) in their Figure 1 showed that the BB peak in Z_H is higher in altitude compared to the BB peak in Z_{DR} whereas in our Figure 3a and 3b the peaks are at similar heights due to the azimuthal averaging. Our datasets show
620 similar signatures as those shown by Brandes and Ikeda (2004) (figures not shown) when the profiles are extracted from slant ranges. Although the BB peaks are not the same in our VPs (or QVPs) due to the azimuthal averaging, the BB boundaries are
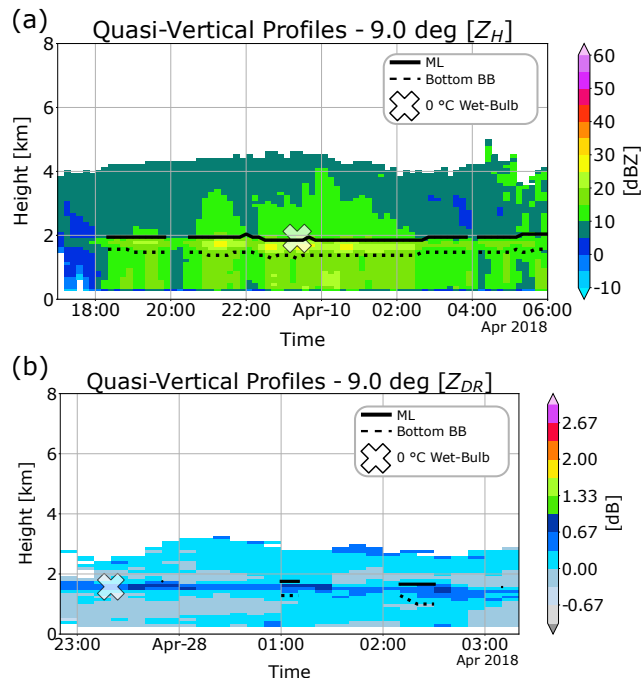
26

(a) Quasi-Vertical Profiles - 9.0 deg $[Z_H]$

(b) Quasi-Vertical Profiles - 9.0 deg $[Z_{DR}]$

Figure 13. Comparison of the ~~FLA~~ MLA outputs ~~at~~ based on the variable P_{10} for QVPs constructed from 9° elevation angle ~~using two different variables: scans.~~ (a) ~~and (b) show~~ shows the ~~performance~~ detection of the ~~variable P_{10}~~ melting layer for a stratiform ~~(top left) and a convective~~ event ~~(top right)~~displayed over an HTI plot of Z_H; (~~c~~b) ~~and (d) display~~ shows the performance ~~of the variable P_{14}~~ for a ~~stratiform (bottom left) and a~~ convective event ~~(bottom right)~~displayed over an HTI plot of Z_{DR}.

on average at similar heights, hence not being a major problem for implementing the MLA.

From the analysis of the QVPs and VPs, we observed that Z_H is ~~the variable that is most~~ a variable susceptible to the different types of precipitation on both ~~types of profiles~~VPs and QVPs, allowing the characterisation of the rain profiles, as previously

625 explored by Fabry and Zawadzki (1995), Kitchen et al. (1994) and Klaassen (1988). Nevertheless, this also accentuates the trouble ~~on the detection of the FL~~ of detecting the ML based only on the reflectivity profiles~~, although some authors, e. g. Gourley and Calvert (2003) developed methods based mainly on this variable.~~. This emphasises the need to incorporate other polarimetric variables ~~to~~into the analysis.

Regarding Z_{DR}, this variable raises several questions about its potential to ~~estimate the FL~~detect the ML. Z_{DR} is a polarimetric

630 variable prone to calibration errors (Vivekanandan et al., 2003), and our datasets are not the exception, as shown in Figure 2c. We decided not to carry out a calibration process at this point, because knowledge of the ~~FL height~~ melting layer boundaries is necessary, as suggested by Gorgucci et al. (1999), Gourley et al. (2009) or Park et al. (2005). Moreover, the values of Z_{DR} ~~greatly~~ vary regarding the elevation angle, as shown in Figures 2c and 2d and proved by Ryzhkov et al. (2005), where they found that Z_{DR} decrease with elevation angles for weather targets. Regardless of these drawbacks, the profiles of Z_{DR} show its

635 sensitivity to the variance on the hydrometeor characteristics as can be seen in Figure 3b, enabling the ~~estimation of the FL.This~~

~~was explored by Brandes and Ikeda (2004), Giangrande et al. (2008), Matrosov et al. (2007), Wolfensberger et al. (2016) and although some of them decided not to include this variable into their algorithms, we included it into the analysis to explore its effectiveness for the FL estimation.~~detection of the ML when using a normalised version.

On the other hand, ρ_{HV} stands out as a tell-tale of the ML, on both QVPs and VPs, as shown in Figures 2e, 2f and 3c. This

640 agrees with the findings of Brandes and Ikeda (2004), Matrosov et al. (2007), Shusse et al. (2011) ~~and Tabary et al. (2006), that based their algorithms~~partially or solely on this polarimetric variableTabary et al. (2006) or Wolfensberger et al. (2016), that included ρ_{HV} into their algorithms. Also, we analysed the quality of the radar datasets on several ~~convective and stratiform rain~~ events based on this variable and found that ρ_{HV} in the rain medium is around 0.99 ~~and~~ so the quality of this variable is reliable for further processing.

645 For our datasets, Φ_{DP} ~~stands out as the profile where the phase of the hydrometeors yields in~~ profiles show complex signatures that are difficult to classify, as shown in Figure 3d. Since the elevation angles used for the construction of the QVPs are below $10°$, the peaks in Φ_{DP} related to the ~~ML~~ melting layer are weak and not well defined~~, although~~. However, when using higher elevation angles ~~,~~the peak in Φ_{DP} should increase, as shown by Trömel et al. (2014). There are also other peaks present at the top of the QVPs, but these peaks ~~are likely~~ may be related to the dendritic growth layer~~(Kaltenboeck and Ryzhkov, 2017)~~

650 , as explored by Kaltenboeck and Ryzhkov (2017). Additionally, the VPs of Φ_{DP} presented in Figure 3d differs ~~to~~ from the profiles showed by Brandes and Ikeda (2004) as in their Figure 1, Φ_{DP} increase on the ML, but for our VPs, there is an inverse peak caused by the ML. Once again, this is related to the averaging process when constructing our profiles.
~~Finally, the fall velocity of hydrometeors has been widely used on several algorithms for the ML characterisation (Baldini and Gorgucci, 20~~
~~. In most of the cases, the velocity profiles are used in combination with other variables (reflectivity, wind profilers data~~

655 ~~and Doppler velocity width) to estimate the height of the FL, but these data are not available on the UKMO weather radar network.As can be seen in Figure 2i~~Finally, the Doppler velocity profiles ~~displayed in the height-versus-time format are~~ prove to be a great tool to ~~observe~~ monitor the development of ~~the~~ precipitation events as ~~they~~ this variable describe the increase of the fall velocity of hydrometeors~~as the snowflakes melt into raindrops. Also, there is~~. Height-versus-Time plots of these profiles show an area where the velocity is nearly zero, describing the shift between ice, snow and melting particles. ~~Hence,~~

660 ~~to take advantage of these measurements~~, as shown in Figure 2i. However, it is not easy to incorporate this variable to an automated peak-detection algorithm. Hence, we propose a simple but effective way to incorporate this variable into the ~~FL~~ML estimation, computing the ~~derivative of the profile(as described in Section ??), that~~ profile's derivative. The proposed method transforms the profile into a similar ~~format of the polarimetric variables that enable the addition of this profile~~shape of the rest of the polarimetric variables to enable its incorporation into an automated peak-detection algorithm, as can be seen in Figures

665 2j and 3e (dotted line).
~~These signatures on the polarimetric profiles and in combination with the radiosonde datasets helped us to corroborate that the top of the ML is related to the $0°C$ isotherm (FL) and we also observed that the bottom of the ML is related to the beginning of the rain region, especially in stratiform precipitation as can be seen in Figures 2 and 3 and demonstrated by previous studies (Brandes and Ikeda, 2004; Kumjian and Lombardo, 2017; Rico-Ramirez et al., 2007; Ryzhkov et al., 2016).Based on all the different~~

670 ~~signatures observed in the ML, we designed an algorithm that detects the strong gradients in the profiles caused by the ML~~

~~to estimate the FL. The algorithm is based on the method proposed by Wolfensberger et al. (2016), where the combination of polarimetric profiles enables the detection of the FL. We modified their algorithm to include all combinations of polarimetric variables to evaluate the capability of each variable and improve the accuracy of the FL estimation. We proposed a method that considers the ML and its boundaries as peaks and valleys within a profile and then enhancing them enables accurate detection of the FL. This is a simple method that differs from previous studies where the ML and its boundaries are detected by complex methods that compute second-order statistics of polarimetric profiles (Baldini and Gorgucci, 2006), assume idealised profiles (Brandes and Ikeda, 2004), use a curvature detection method (Fabry and Zawadzki, 1995) or methods that rotate the coordinate system to locate the ML boundaries (Rico-Ramirez and Cluckie, 2007). Moreover, some of these methods are tailored exclusively to a specific scanning strategy or type of profiles, so we proposed two parameters (k and w) intended to be calibrated depending on the type of profiles.~~We also assessed the consistency between QVPs and VPs of Z_H to make sure that the low-elevation angles available in our datasets are still useful to compute reliable QVPs, as Ryzhkov et al. (2016) suggested that QVPs should be built from data collected at higher elevation angles that exceed $20°$. The results for the lower elevation angles ($4°$ and $6°$) agree with the findings by Ryzhkov et al. (2016) proving that decreasing the antenna elevation degrades the resolution of the QVPs. However, the QVPs collected at $9°$ elevation angles are still in good agreement with the VPs of Z_H; in overall, there is a good agreement between datasets in stratiform events as the correlation coefficient is close to 0.7, but in convective events, the differences between the profiles increase, as can be seen in Figure 6 and Figure 7. Therefore, we concluded that the QVP can be generated from elevation scans of $9°$ as the effects of beam broadening and horizontal inhomogeneity are not as pronounced as expected and this enables the use of these QVPs of polarimetric variables for the ~~detection of the FL.~~ ML detection .

Based on all the different signatures triggered by the melting layer, we designed an algorithm that detects strong gradients within a profile resulting from the combination of several radar measurements. The algorithm is based on the method proposed by Wolfensberger et al. (2016), but it was modified to include all the combinations of polarimetric variables and evaluate their capabilities to detect the melting layer boundaries. Also, we propose a simple method to enhance the peaks within the profiles to refine the detection of the ML. This method differs from previous studies where the melting layer and its boundaries are detected by complex methods that compute second-order statistics of polarimetric profiles (Baldini and Gorgucci, 2006), assume idealised profiles (Brandes and Ikeda, 2004), use a curvature detection method (Fabry and Zawadzki, 1995) or methods that rotate the coordinate system to locate the melting layer boundaries (Rico-Ramirez and Cluckie, 2007). The results of the ~~FLA~~ MLA were validated by comparing ~~with the measured FL height (FL_{RS}) from radiosonde data~~ them with heights of $0°C$ wet-bulb isotherms. Using this data, we demonstrated the potential of each one of the polarimetric variables to ~~estimate the FL~~ detect the ML, by presenting performance metrics of ~~all the available variables and type of profiles~~ the computed profiles and its combinations, as shown in Sections ~~?? and ??~~ 5.2 and 5.3. For the VPs, we demonstrated that the proposed profile $gradV$ is helpful for the ~~estimation of the FL (see Figures 10c and 10d~~ detection of the ML (see Figure 8), especially in combination with other variables, e.g. $P_{26} = [Z_H^* \cdot (1 - \rho_{HV}^*) \cdot (1 - gradV^*)]$ ~~that generate accurate estimations of the FL~~ accurately outlines the melting layer, regardless if it was applied to convective or stratiform events. ~~It is worth noting that the combination P_{10} is similar to the algorithm proposed by Wolfensberger et al. (2016) (although the refinement process of the estimation of the~~

FL is different). ~~However, in our case, it showed less accuracy, especially when the profiles were related to convective-type events, as shown in Figures 13c and 13d. Regarding the bottom of the ML~~Regarding the melting layer bottom, it is important to ~~highlight~~ stress that only a visual assessment enables the validation of the performance of the algorithm ~~in this matter~~on this matter, but as shown in Figure 10, the proposed variable steadily demarcates the boundaries of the melting layer.

710 On the other hand, ~~for the QVPs, the incorporation of~~ when applying the algorithm to QVPs, adding Z_{DR} ~~into the algorithm showed to add valuable information to the identification and characterisation~~ to the analysis provided valuable information for the identification of the ML. Hence the combination P_{14} is selected as the ~~one with the best performance for the detection of the FL when applied to the QVPs. As can be seen~~ best predictor of the ML. As shown in Figure 11, the accuracy improves ~~in comparison to the profile P_{10} that only includes the combination of~~ compared to profiles that only include Z_H^* and $1 - \rho_{HV}^*$.

715 Also, this variable adequately delimits the melting layer especially for stratiform events and also detects the melting layer signatures in convective events, as shown in Figure 13.

Therefore, we ~~select~~ selected these two profiles P_{14} and P_{26} for QVPs and VPs, respectively, as the combinations that achieve the higher accuracy on the ~~estimation of the FL~~ detection of the ML and, at a certain degree, the ~~ML~~ melting layer characterisation. These combinations proved to be accurate, with an average error close to the resolution of the radar and the mismatch

720 in time and space. The proposed algorithm produces errors within 200m in the ~~estimation of the FL estimation, which is~~ ML estimation, consistent with previous work ~~(Brandes and Ikeda, 2004; Baldini and Gorgucci, 2006; Kitchen et al., 1994; Wolfensberger et al~~ as Brandes and Ikeda (2004); Baldini and Gorgucci (2006); Kitchen et al. (1994); Wolfensberger et al. (2016). Finally, it is worth noting that the algorithm enables the detection of the ~~FL~~ML based on radar measurements only, without relying on ~~FL estimations~~ data generated from NWP model runs. This allows the implementation of radar rainfall correction schemes ~~or~~

725 ~~hydrometeor classification algorithms~~ based on radar measurements only.

7 Conclusions

In this paper, we generated QVPs and VPs of polarimetric variables collected by an operational C-band radar to explore the ~~identification of the FL. We observed that QVPs of polarimetric radar variables reveal signatures that~~ melting layer signatures. These signatures are difficult to observe in ~~traditional PPI scans~~the traditional PPI format. Also, ~~QVPs show more precipitation~~

730 the QVPs represent bigger spatial-distributed events than VPs as the VPs can only measure events that are effectively happening above the radar. Even more, for the datasets used in this work, scans taken at $90°$ elevation presents limitations when reading data on the first kilometre due to technical restrictions, this situation restrain the observation of rainfall features at relative lower heights, while ~~the~~ QVPs are not affected by this constraint.

We performed a numerical comparison of the VP and QVPs of reflectivity to demonstrate the consistency of the measurements

735 involving the elevation angle of the scans. The analysis shows that QVPs generated using elevation angles at $9°$ exhibit good agreement with VPs ($r \sim 0.7$) while elevations below this elevation increase the discrepancy with vertical scans and are not suitable for the detection of the ~~FL~~ML.

We analysed the signatures of the polarimetric variables to characterise the ~~ML~~ melting layer because they represent a diversity

of ~~orientation, shape, size, and~~ microphysical processes of the hydrometeors, and we concluded that these features have an

740 impact on the shape of the polarimetric profiles and therefore can improve the detection of the ~~FL~~ML.

We developed a robust, operational ~~FLA~~ MLA that detects the signatures of the ~~ML~~ melting layer using polarimetric QVPs and VPs. The fundamentals of the design of the ~~FLA are: A~~ MLA are: (i) a simple method to detect peaks and valleys within the profiles; ~~The~~ (ii) the combination of normalised variables ~~; And~~ and (iii) the incorporation of two parameters (k and w) that can be calibrated depending on the characteristics and type of the profiles.~~We propose a novel~~

745 We proposed a profile $[gradV]$ for velocities taken at vertical incidence, that proves to be a helpful variable for the ~~FL estimation.We demonstrated the capability~~ ML estimation.

We showed the capabilities of all the ~~available VPs and QVPs of radar variables for the estimation of the FL~~radar variables and its combinations to detect the ML, providing individual performance metrics and analysing their performance on convective and stratiform events. For VPs, the combination P_{26}, that use the normalised version of the reflectivity, the correlation coeffi-

750 cient and the gradient of the velocity, i.e. $[Z_H^* \cdot (1 - \rho_{HV}^*) \cdot (1 - gradV^*)]$ achieve ~~accurate estimations of the FL~~an accurate detection of the ML. For QVPs, the combination ~~$P_{14} = [Z_H^* \cdot (Z_{DR}^* \cdot (1 - \rho_{HV}^*)]$~~ $P_{14} = [Z_H^* \cdot (Z_{DR}^*) \cdot (1 - \rho_{HV}^*)]$ is selected as the combination that ~~produces better results for the FL estimation on both, stratiform and convective events~~better detects the melting layer boundaries.

The ~~FLA proves~~ MLA proved to be accurate as the errors $(MAE, RMSE)$ between the selected outputs of the ~~FLA~~ MLA

755 and the data collected by radiosonde are close to 200 m.

31

765   facilities of the Advanced Computing Research Centre, University of Bristol

(http://www.bris.ac.uk/acrc/).

References

American Meteorological Society: Melting layer. Glossary of Meteorology, https://glossary.ametsoc.org/wiki/Melting_layer, 2021a.

American Meteorological Society: Melting level. Glossary of Meteorology, https://glossary.ametsoc.org/wiki/Melting_level, 2021b.

770 Baldini, L. and Gorgucci, E.: Identification of the melting layer through dual-polarization radar measurements at vertical incidence, Journal of Atmospheric and Oceanic Technology, 23, 829–839, https://doi.org/10.1175/JTECH1884.1, 2006.

Bechini, R., Baldini, L., Cremonini, R., and Gorgucci, E.: Differential reflectivity calibration for operational radars, Journal of Atmospheric and Oceanic Technology, 25, 1542–1555, https://doi.org/10.1175/2008JTECHA1037.1, 2008.

Boodoo, S., Hudak, D., Donaldson, N., and Leduc, M.: Application of dual-polarization radar melting-layer detection algorithm, Journal of
775 Applied Meteorology and Climatology, 49, 1779–1793, https://doi.org/10.1175/2010JAMC2421.1, 2010.

Brandes, E. A. and Ikeda, K.: Freezing-level estimation with polarimetric radar, Journal of Applied Meteorology, 43, 1541–1553, https://doi.org/10.1175/JAM2155.1, 2004.

Bringi, V. N., Chandrasekar, V., Balakrishnan, N., and Zrnić, D. S.: An Examination of Propagation Effects in Rainfall on Radar Measurements at Microwave Frequencies, https://doi.org/10.1175/1520-0426(1990)007<0829:aeopei>2.0.co;2, 1990.

780 Bringi, V. N., Keenan, T. D., and Chandrasekar, V.: Correcting C-band radar reflectivity and differential reflectivity data for rain attenuation: A self-consistent method with constraints, IEEE Transactions on Geoscience and Remote Sensing, 39, 1906–1915, https://doi.org/10.1109/36.951081, 2001.

Cheng, M. and Collier, C. G.: An Objective Method for Recognizing and Partially Correcting Brightband Error in Radar Images, Journal of Applied Meteorology, 32, 1142–1149, https://doi.org/10.1175/1520-0450(1993)032<1142:AOMFRA>2.0.CO;2, 1993.

785 Collier, C. G.: On the formation of stratiform and convective cloud, Weather, 58, 62–69, https://doi.org/10.1256/wea.239.02, 2003.

Dance, S. L., Ballard, S. P., Bannister, R. N., Clark, P., Cloke, H. L., Darlington, T., Flack, D. L., Gray, S. L., Hawkness-Smith, L., Husnoo, N., Illingworth, A. J., Kelly, G. A., Lean, H. W., Li, D., Nichols, N. K., Nicol, J. C., Oxley, A., Plant, R. S., Roberts, N. M., Roulstone, I., Simonin, D., Thompson, R. J., and Waller, J. A.: Improvements in forecasting intense rainfall: Results from the FRANC (Forecasting Rainfall exploiting new data Assimilation techniques and Novel observations of Convection) project, Atmosphere, 10,
790 https://doi.org/10.3390/atmos10030125, 2019.

Darlington, T.: Met Office, (Personal communication), 2019.

Fabry, F.: Radar meteorology: principles and practice, Cambridge University Press, Cambridge, United Kingdom, 2015.

Fabry, F. and Zawadzki, I.: Long-term radar observations of the melting layer of precipitation and their interpretation, https://doi.org/10.1175/1520-0469(1995)052<0838:LTROOT>2.0.CO;2, 1995.

795 Giangrande, S. E., Krause, J. M., and Ryzhkov, A. V.: Automatic designation of the melting layer with a polarimetric prototype of the WSR-88D radar, Journal of Applied Meteorology and Climatology, 47, 1354–1364, https://doi.org/10.1175/2007JAMC1634.1, 2008.

Gorgucci, E., Scarchilli, G., and Chandrasekar, V.: A procedure to calibrate multiparameter weather radar using properties of the rain medium, IEEE Transactions on Geoscience and Remote Sensing, 37, 269–276, https://doi.org/10.1109/36.739161, 1999.

Gourley, J. J. and Calvert, C. M.: Automated detection of the bright band using WSR-88D data, Weather and Forecasting, 18, 585–599,
800 https://doi.org/10.1175/1520-0434(2003)018<0585:ADOTBB>2.0.CO;2, 2003.

Gourley, J. J., Illingworth, A. J., and Tabary, P.: Absolute calibration of radar reflectivity using redundancy of the polarization observations and implied constraints on drop shapes, Journal of Atmospheric and Oceanic Technology, 26, 689–703, https://doi.org/10.1175/2008JTECHA1152.1, 2009.

Griffin, E. M., Schuur, T. J., and Ryzhkov, A. V.: A polarimetric analysis of ice microphysical processes in snow, using quasi-vertical profiles, Journal of Applied Meteorology and Climatology, 57, 31–50, https://doi.org/10.1175/JAMC-D-17-0033.1, 2018.

Hall, W., Rico-Ramirez, M. A., and Krämer, S.: Classification and correction of the bright band using an operational C-band polarimetric radar, Journal of Hydrology, 531, 248–258, https://doi.org/10.1016/j.jhydrol.2015.06.011, 2015.

Harrison, D. L., Driscoll, S. J., and Kitchen, M.: Improving precipitation estimates from weather radar using quality control and correction techniques, Meteorological Applications, 7, 135–144, https://doi.org/10.1017/S1350482700001468, 2000.

Hong, Y. and Gourley, J. J.: Radar hydrology: principles, models, and applications, Taylor & Francis, Boca Raton, 2015.

Islam, T. and Rico-Ramirez, M. A.: An overview of the remote sensing of precipitation with polarimetric radar, Progress in Physical Geography, 38, 55–78, https://doi.org/10.1177/0309133313514993, 2014.

Islam, T., Rico-Ramirez, M. A., Han, D., and Srivastava, P. K.: Sensitivity associated with bright band/melting layer location on radar reflectivity correction for attenuation at C-band using differential propagation phase measurements, Atmospheric Research, 135-136, 143–158, https://doi.org/10.1016/j.atmosres.2013.09.003, http://dx.doi.org/10.1016/j.atmosres.2013.09.003, 2014.

Kaltenboeck, R. and Ryzhkov, A.: A freezing rain storm explored with a C-band polarimetric weather radar using the QVP methodology, Meteorologische Zeitschrift, 26, 207–222, https://doi.org/10.1127/metz/2016/0807, 2017.

Kitchen, M., Brown, R., and Davies, A. G.: Real-time correction of weather radar data for the effects of bright band, range and orographic growth in widespread precipitation, Quarterly Journal of the Royal Meteorological Society, 120, 1231–1254, https://doi.org/10.1002/qj.49712051906, 1994.

Klaassen, W.: Radar Observations and Simulation of the Melting Layer of Precipitation, Journal of the Atmospheric Sciences, 45, 3741–3753, https://doi.org/10.1175/1520-0469(1988)045<3741:ROASOT>2.0.CO;2, 1988.

Kumjian, M.: Principles and applications of dual-polarization weather radar. Part I: Description of the polarimetric radar variables, Journal of Operational Meteorology, 1, 226–242, https://doi.org/10.15191/nwajom.2013.0119, 2013a.

Kumjian, M.: Principles and applications of dual-polarization weather radar. Part II: Warm- and cold-season applications, Journal of Operational Meteorology, 1, 243–264, https://doi.org/10.15191/nwajom.2013.0120, http://nwafiles.nwas.org/jom/articles/2013/2013-JOM20/2013-JOM20.pdf, 2013b.

Kumjian, M. R. and Lombardo, K. A.: Insights into the evolving microphysical and kinematic structure of northeastern U.S. winter storms from dual-Polarization doppler radar, Monthly Weather Review, 145, 1033–1061, https://doi.org/10.1175/MWR-D-15-0451.1, 2017.

Matrosov, S. Y., Clark, K. A., and Kingsmill, D. E.: A polarimetric radar approach to identify rain, melting-layer, and snow regions for applying corrections to vertical profiles of reflectivity, Journal of Applied Meteorology and Climatology, 46, 154–166, https://doi.org/10.1175/JAM2508.1, 2007.

Met Office: Met Office Herstmonceux station high resolution radiosonde data. NCAS British Atmospheric Data Centre, https://catalogue.ceda.ac.uk/uuid/51b40654ef68462c818677963651a7bb, 2007.

Met Office: Chenies C-band rain radar dual polar products. NCAS British Atmospheric Data Centre, https://catalogue.ceda.ac.uk/uuid/bb3c55e36b4a4dc8866f0a06be3d475b, 2013.

Mittermaier, M. P. and Illingworth, A. J.: Comparison of model-derived and radar-observed freezing-level heights: Implications for vertical reflectivity profile-correction schemes, Quarterly Journal of the Royal Meteorological Society, 129, 83–95, https://doi.org/10.1256/qj.02.19, 2003.

Moin, P.: Fundamentals of Engineering Numerical Analysis, Cambridge University Press, Cambridge, https://doi.org/10.1017/CBO9780511781438, 2010.

Norman, K., Sugier, J., Edwards, M., Darlington, T., Lissaman, V., Riley, R., Kitchen, M., Husnoo, N., and Georgiou, S.: Renewing the UK weather radar network, in: Regional Meeting - British Hydrological Society South West Section, Bristol, 2014.

Park, H. S., Ryzhkov, A. V., Zrnić, D. S., and Kim, K. E.: The hydrometeor classification algorithm for the polarimetric WSR-88D: Description and application to an MCS, Weather and Forecasting, 24, 730–748, https://doi.org/10.1175/2008WAF2222205.1, 2009.

Park, S. G., Bringi, V. N., Chandrasekar, V., Maki, M., and Iwanami, K.: Correction of radar reflectivity and differential reflectivity for rain attenuation at X band. Part I: Theoretical and empirical basis, Journal of Atmospheric and Oceanic Technology, 22, 1621–1632, https://doi.org/10.1175/JTECH1803.1, 2005.

Richardson, L. M., Zitte, W. D., Lee, R. R., Melnikov, V. M., Ice, R. L., and Cunningham, J. G.: Bragg scatter detection by the WSR-88D. Part II: Assessment of ZDR bias estimation, Journal of Atmospheric and Oceanic Technology, 34, 479–493, https://doi.org/10.1175/JTECH-D-16-0031.1, 2017.

Rico-Ramirez, M. A.: Adaptive attenuation correction techniques for C-band polarimetric weather radars, IEEE Transactions on Geoscience and Remote Sensing, 50, 5061–5071, https://doi.org/10.1109/TGRS.2012.2195228, 2012.

Rico-Ramirez, M. A. and Cluckie, I. D.: Bright-band detection from radar vertical reflectivity profiles, International Journal of Remote Sensing, 28, 4013–4025, https://doi.org/10.1080/01431160601047797, 2007.

Rico-Ramirez, M. A. and Cluckie, I. D.: Classification of ground clutter and anomalous propagation using dual-polarization weather radar, IEEE Transactions on Geoscience and Remote Sensing, 46, 1892–1904, https://doi.org/10.1109/TGRS.2008.916979, 2008.

Rico-Ramirez, M. A., Cluckie, I. D., Shepherd, G., and Pallot, A.: A high-resolution radar experiment on the island of Jersey, Meteorological Applications, 14, 117–129, https://doi.org/10.1002/met.13, 2007.

Ryzhkov, A., Zhang, P., Reeves, H., Kumjian, M., Tschallener, T., Trömel, S., and Simmer, C.: Quasi-vertical profiles-A new way to look at polarimetric radar data, Journal of Atmospheric and Oceanic Technology, 33, 551–562, https://doi.org/10.1175/JTECH-D-15-0020.1, 2016.

Ryzhkov, A. V., Giangrande, S. E., Melnikov, V. M., and Schuur, T. J.: Calibration issues of dual-polarization radar measurements, Journal of Atmospheric and Oceanic Technology, 22, 1138–1155, https://doi.org/10.1175/JTECH1772.1, 2005.

Sánchez-Diezma, R., Zawadzki, I., and Sempere-Torres, D.: Identification of the bright band through the analysis of volumetric radar data, Journal of Geophysical Research: Atmospheres, 105, 2225–2236, https://doi.org/10.1029/1999JD900310, 2000.

Shusse, Y., Takahashi, N., Nakagawa, K., Satoh, S., and Iguchi, T.: Polarimetric radar observation of the melting layer in a convective rainfall system during the rainy season over the East China Sea, Journal of Applied Meteorology and Climatology, 50, 354–367, https://doi.org/10.1175/2010JAMC2469.1, 2011.

Smyth, T. J. and Illingworth, A. J.: Radar estimates of rainfall rates at the ground in bright band and non-bright band events, Quarterly Journal of the Royal Meteorological Society, 124, 2417–2434, https://doi.org/10.1256/smsqj.55111, 1998.

Tabary, P., Henaff, A. L., Vulpiani, G., Parent du Chatelet, J., and Gourley, J. J.: Melting layer characterization and identification with a C-band dual-polarization radar : a long-term analysis., in: Fourth European Conference on Radar in Meteorology and Hydrology, 2006.

Trömel, S., Ryzhkov, A. V., Zhang, P., and Simmer, C.: Investigations of backscatter differential phase in the melting layer, Journal of Applied Meteorology and Climatology, 53, 2344–2359, https://doi.org/10.1175/JAMC-D-14-0050.1, 2014.

Vignal, B., Andrieu, H., and Creutin, J. D.: Identification of vertical profiles of reflectivity from volume scan radar data, Journal of Applied Meteorology, 38, 1214–1228, https://doi.org/10.1175/1520-0450(1999)038<1214:IOVPOR>2.0.CO;2, 1999.

Vivekanandan, J., Zhang, G., Ellis, S. M., Rajopadhyaya, D., and Avery, S. K.: Radar reflectivity calibration using differential propagation phase measurement, Radio Science, 38, 1–14, https://doi.org/10.1029/2002rs002676, 2003.

880 White, A. B., Gottas, D. J., Strem, E. T., Ralph, F. M., and Neiman, P. J.: An automated brightband height detection algorithm for use with Doppler radar spectral moments, Journal of Atmospheric and Oceanic Technology, 19, 687–697, https://doi.org/10.1175/1520-0426(2002)019<0687:AABHDA>2.0.CO;2, 2002.

Wolfensberger, D., Scipion, D., and Berne, A.: Detection and characterization of the melting layer based on polarimetric radar scans, Quarterly Journal of the Royal Meteorological Society, 142, 108–124, https://doi.org/10.1002/qj.2672, 2016.